Palaeontologia Electronica
palaeo-electronica.org

A reinterpretation and taxonomic revision of *Ultrastenos willisi* Stein, Hand and Archer, 2016, a short-snouted mekosuchine crocodylian from the Oligocene of northern Australia

Adam M. Yates and Michael Stein

ABSTRACT

Ultrastenos willisi from the Oligocene of the Riversleigh World Heritage Area, was described as a mekosuchine crocodylian with a gavial-like, longirostrine morphology. However, the rostrum is not preserved, and the reconstruction rests on a set of inferences that are based on the shape of a mandibular fragment and a cranial reconstruction that was assembled from non-joining fragments. Contrasting with the reconstruction are the proportionally small supratemporal fenestrae and the blunt, molariform posterior teeth, which are discordant with the slender longirostrine morphotype. The issue is resolved by the discovery that QM F31076, a posterior skull fragment ('White Hunter cranial form 1'), which has been referred to *U. willisi*, is likely to be the missing posterior end of the extremely brevirostrine holotype of *'Baru' huberi*. QM F31076 'White Hunter cranial form 1' can be further linked to the holotype of *'B'. huberi* via their matching size, preservation and dermal ornamentation. 'White Hunter cranial form 1', in turn, shares a combination of cranial apomorphies with *U. willisi* and belongs to the same species, indicating that *U. willisi* is a junior subjective synonym of *'B'. huberi.* However, previous phylogenetic analyses have found that *'Baru' huberi* is more closely related to other mekosuchine genera than it is to *Baru*. Consequently, *Ultrastenos* is retained as a valid genus, and the new combination *Ultrastenos huberi* is established. With the discovery that *Ultrastenos* is not a longirostrine taxon there are no longer any known longirostrine mekosuchines, suggesting that the otherwise disparate Mekosuchinae failed to occupy this region of morphospace.

Adam M. Yates. Megafauna Central, Museum and Art Gallery of the Northern Territory, Alice Springs, Northern Territory, Australia. (corresponding author). adamm.yates@magnt.net.au
ORCID: 0000-0003-3568-2585
Michael Stein. Earth and Sustainability Science Research Center, University of New South Wales, Sydney, New South Wales, Australia. michael@davidstein.com.au

Key words: *Ultrastenos*; Mekosuchinae; Crocodylia; Oligocene; Australia; ecomorphology

Final citation: Yates, Adam M. and Stein, Michael. 2024. A reinterpretation and taxonomic revision of *Ultrastenos willisi* Stein, Hand and Archer, 2016, a short-snouted mekosuchine crocodylian from the Oligocene of northern Australia. Palaeontologia Electronica, 27(1):a22.
https://doi.org/10.26879/1355
palaeo-electronica.org/content/2024/5183-ultrastenos-revised

Copyright: April 2024 Palaeontological Association.
This is an open access article distributed under the terms of the Creative Commons Attribution License, which permits unrestricted use, distribution, and reproduction in any medium, provided the original author and source are credited.
creativecommons.org/licenses/by/4.0

Submission: 6 November 2023. Acceptance: 24 March 2024.

INTRODUCTION

Mekosuchinae is an extinct clade of Australasian crocodylians that are particularly diverse and abundant in the Oligo-Miocene deposits of Queensland and the Northern Territory (Willis et al., 1990; Willis, 1997, 2001; Yates, 2017; Ristevski et al., 2023a). Mekosuchines are remarkable in that they present a number of distinct ecomorphological types that match, to greater and lesser degrees, the ecomorphological categories of crocodyliforms that have been established on the basis of rostral shape and other correlated skull characters (Busbey, 1995; Brochu, 2001; Drumheller and Wilberg, 2020). Basal genera such as *Australosuchus* Willis and Molnar, 1991a, *Kambara* Willis et al., 1993, and *Kalthifrons* Yates and Pledge, 2017, have moderately elongate (mesorostrine), dorsoventrally flattened (platyrostral) rostra that are broad-based and roughly triangular in dorsal view. These fit the generalist category of Drumheller and Wilberg (2020). *Quinkana* Molnar, 1982, have mesorostrine, deeply vaulted (altirostral), often slab-sided rostra with reduced undulations of the tooth row ("festooning") and fully ziphodont teeth. These fit the ziphodont category (Brochu, 2001; Drumheller and Wilberg, 2020), which are suggested to have been terrestrial predators (Molnar, 1982; Rossmann, 2000; Brochu, 2012). *Paludirex* Ristevski et al., 2020, has a brevirostrine, platyrostral rostrum that is closer to U-shaped than to triangular. This genus fits into the macro-generalist category (Drumheller and Wilberg, 2020), which is supported by the extreme heterodonty of *Paludirex* and the enormous size of the enlarged teeth of the canine peaks. *Baru* Willis et al., 1990, presents another genus of mekosuchines that are probably specialized for taking prey as large, or larger, than its own body size. However, its morphology differs from the other taxa that Drumheller and Wilberg (2020) place in the macro-generalist category in that the maxillary rostrum is triangular in dorsal view and altirostral in lateral view. *Mekosuchus* Balouet and Buffetaut, 1987, and *Trilophosuchus* Willis, 1993, are mekosuchine genera with very small skull size and probable extreme brevirostry. The ecology of these dwarf taxa is unclear, they are usually supposed to be at least partly terrestrial (Willis, 2001; Scanlon, 2014; Stein et al., 2016a; Ristevski, 2022a, b), and the possibility that they were even arboreal has been suggested in the non-technical literature (Willis, 1995). Lastly, we can consider *'Baru' huberi* Willis, 1997 (Figure 1A-C). This species is distinctly different from all other known species of *Baru*, indeed Lee and Yates (2018) and Ristevski et al. (2023a) found that it does not form an exclusive clade with other species of *Baru*. Not only is *'B.' huberi* much smaller than other species of *Baru* (the estimated skull length of the holotype is 200 mm), but it also has a platyrostral and extremely brevirostrine skull (rostral proportion, sensu Erickson et al., 2012, = 0.93). Based on skull shape it would appear to fall within the brevirostrine heterodont category of Drumheller and Wilberg (2020), although it lacked the extreme heterodonty shown by other members of this category.

With this degree of morphological disparity among mekosuchines, it is perhaps surprising that the slender longirostrine category is at best poorly represented, indeed probably unrepresented within the clade. This category, which is typified by gavialids, has evolved multiple times amongst Crocodyliformes (Ballell et al., 2019; Drumheller and Wilberg, 2020) but there are only two candidate taxa among all named potential mekosuchines, namely *Harpacochampsa camfieldensis* Megirian et al., 1991, and *Ultrastenos willisi* Stein et al., 2016b (Figure 2A-J).

The systematic position of the first of these, *H. camfieldensis*, from the Middle Miocene of Bullock Creek in the Northern Territory, remains controversial, and it is probably not a mekosuchine (Lee and Yates, 2018; Ristevski et al., 2020, 2021, 2023a, b).

The only other proposed slender longirostrine mekosuchine is *U. willisi*, from the late Oligocene of the Riversleigh World Heritage Area of Queensland (Stein et al., 2016b). This species was based on QM F42665, a fragmentary skull and mandible with associated postcrania from the Low Lion Site (Stein et al., 2016b), which has produced mammalian taxa belonging to the Riversleigh faunal zone A (Gillespie et al., 2019). Riversleigh Faunal Zone A is dated to the Late Oligocene (Archer et al., 1997; Myers and Archer, 1997; Travouillon et al., 2006; Arena et al., 2015; Myers et al., 2017). The mekosuchinae status of *Ultrastenos* is not in dispute, and Rio and Mannion (2021) found it to nest close to *Mekosuchus* itself. However, it may not be a slender longirostrine.

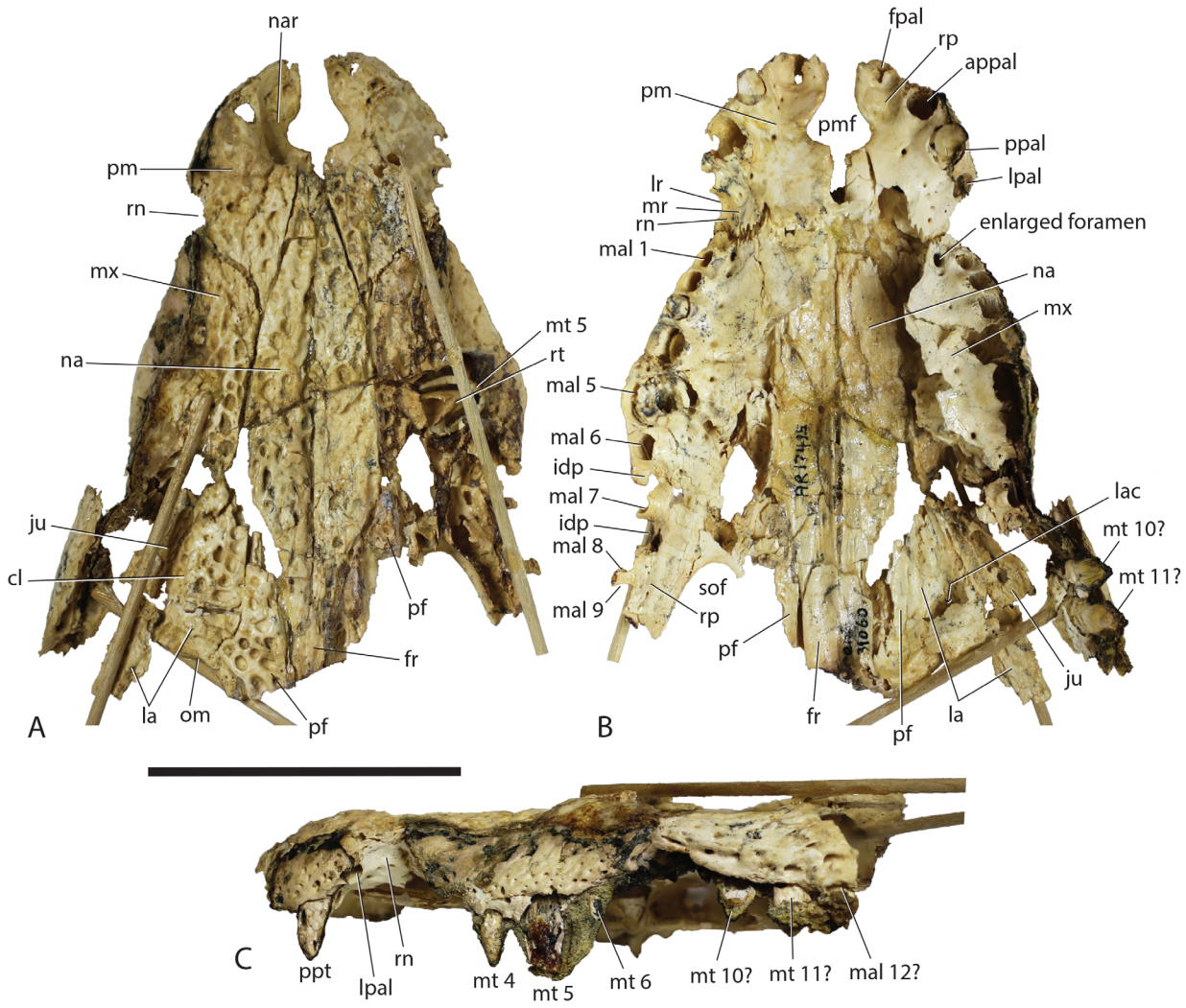

FIGURE 1. *Ultrastenos huberi,* QM F31060, holotype, maxillary rostrum. A, dorsal view. B, ventral view. C, left lateral view. Abbreviations: appal, antepenultimate premaxillary alveolus; cl, canthus lacrimalis; fpal, first premaxillary alveolus; fr, frontal; idp, interdental reception pit; ju, jugal; lpal, last premaxillary alveolus; la, lacrimal; lac, lacrimal canal; lr, lateral ridge; mal, maxillary alveolus; mt, maxillary tooth; mr, medial ridge; mx, maxilla; na, nasal; nar, naris; om, orbital margin; ppt, penultimate premaxillary tooth; pm, premaxilla; pmf, premaxillary fenestra; pf, prefrontal; rn, reception notch for dentary tooth 4; rp, reception pit; rt, replacement tooth; sof, suborbital fenestra. Note that the premaxillary teeth are not numbered because the loss of a tooth position renders numbering ambiguous. Scale bar equals 50 mm.

The type specimen of *U. willisi* is quite incomplete and lacks any pieces from the pre-orbital region (Figure 2A-J). Thus, the longirostrine reconstruction provided by Stein et al. (2016b) is based upon inferences drawn from the posterior region of the skull and jaws and it is open to argument and reinterpretation.

Included within the hypodigm of *U. willisi* are a pair of incomplete, posterior, cranial specimens (QM F31075 and F31076; Figures 3-5) that had been described by Willis (1997) as 'White Hunter cranial form 1' (hereafter 'WH cranial form 1'). These incomplete skulls came from the White Hunter Site in the Riversleigh World Heritage Area, another site that is part of the late Oligocene Riversleigh Faunal Zone A (Archer et al., 1997; Travouillon et al., 2006). White Hunter Site has produced a remarkably diverse crocodylian fauna (Willis, 1997) and is the type locality for four species: *Mekosuchus whitehunterensis* Willis, 1997, *Quinkana meboldi* Willis, 1997, *Baru wickeni* Willis, 1997 and *'B.' huberi.* Willis (1997) considered that it was likely that 'WH cranial form 1' belonged to one of his four named species but could not positively

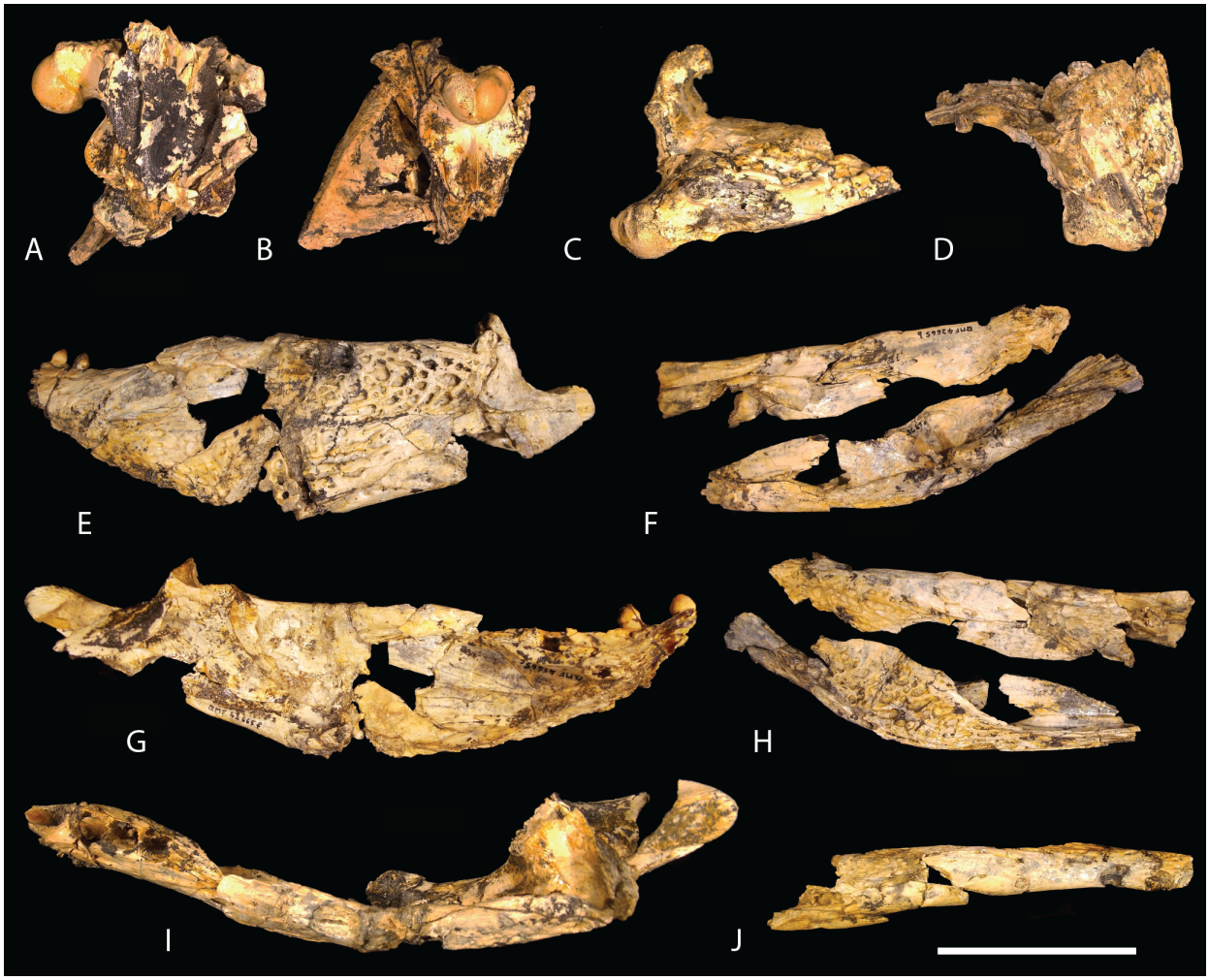

FIGURE 2. *Ultrastenos huberi*, QM F42665, significant fragments of the holotype of *U. willisi* Stein et al. A, B, basicranial fragment with displaced adherent left pterygoid in right lateral (A) and occipital views (B). C, D, right temporal fragment in lateral (C) and dorsal views (D). E, G, I, posterior end of left mandibular ramus in lateral (E), medial (G) and dorsal (I) views. F, H, disarticulated right suranguar and angular in medial (F) and lateral (H) views. J, right surangular in dorsal view (anterior to the left). Scale bar equals 50 mm.

refer it to any of them due to the absence of overlapping parts. Stein et al. (2016b) found the proportions of the reconstructed occiput of *U. willisi* matched those of the braincase of 'WH cranial form 1' as did the lateral margin of the quadrate and therefore referred the unnamed cranial form to their new taxon. If this referral is accepted, as it is in this work, 'WH cranial form 1' becomes very significant in determining the true nature and systematic position of the QM F42665, the holotype of *U. willisi*.

The Case for Longirostry in QM F42665

Stein et al. (2016b) cite the apparent transverse constriction of the dentigerous portion of the mandible relative to the postdentary region as the main support for their slender longirostrine reconstruction of QM F42665. Such a constriction would indicate that the tooth rows were closely spaced and subparallel on a slender anterior mandible. However, QM F42665 does not include articulated left and right dentaries, or any part of the mandibular symphysis. Thus the constriction of the tooth rows cannot be observed directly and has to be inferred from the shape of the incomplete left mandibular ramus and the manner with which it articulates with the reconstructed cranium. When the left articular is placed against the reflected right quadrate of their reconstruction, so that the surangular is aligned with the lateral margin of the quadratojugal and jugal, the medial curvature of the jaw fragment results in the posterior tooth row being placed

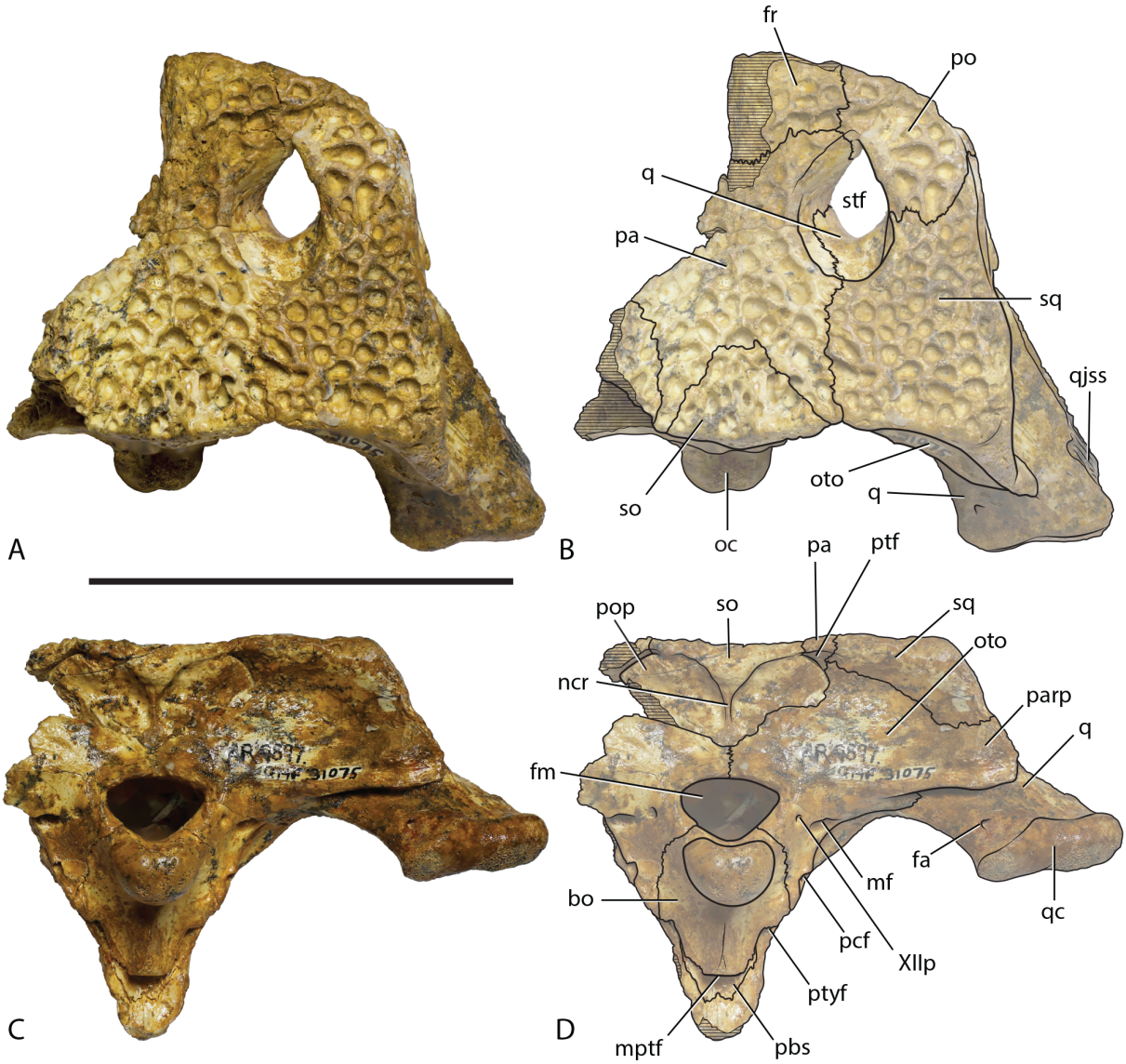

FIGURE 3. *Ultrastenos huberi*, QM F31075, White Hunter Cranial Form 1, posterior cranial fragment. A, B, dorsal view as a photograph (A), and as an annotated photograph with interpretive overlay (B). C, D, occipital view as a photograph (C), and an annotated photograph with interpretive overlay (D). Abbreviations: bo, basioccipital; fa, foramen aereum; fm, foramen magnum; fr, frontal; mf, metotic foramen; mptf, median pharyngeal tube foramen; ncr, nuchal crest; oc, occipital condyle; oto, otoccipital; pa, parietal; parp, paroccipital process; pbs, parabasisphenoid; pcf, posterior carotid foramen; po, postorbital; pop, postoccipital process of the supraoccipital; ptf, posttemporal fenestra; ptyf, pharyngotympanic foramen; q, quadrate; qc, quadrate condyle; qjss, sutural surface for articulation with the quadratougal; so, supraoccipital; sq, squamosal; stf, supratemporal fenestra; XIIp, posterior foramen for cranial nerve XII (posterior hypoglossal foramen). Scale bar equals 50 mm.

two to three centimetres from the midline. From this position the dentary tooth rows would have to continue as elongate closely set, subparallel rows (i.e., an elongate longirostrine rostrum).

As further evidence for longirostry in QM F42665, Stein et al. (2016b) highlighted a set of characteristics of the posterior skull that are thought to be correlated with a slender elongate rostrum. Among these, Stein et al. (2016b) suggested that the mandible was relatively shallow in comparison to other mekosuchines and that its dorsal profile was level, lacking a distinct rise from the dentary onto the surangular (Figure 2E-H). A shallow mandible can be reasonably assumed to correlate with a shallow skull, which is indeed correlated with slender longirostry (Iijima, 2017).

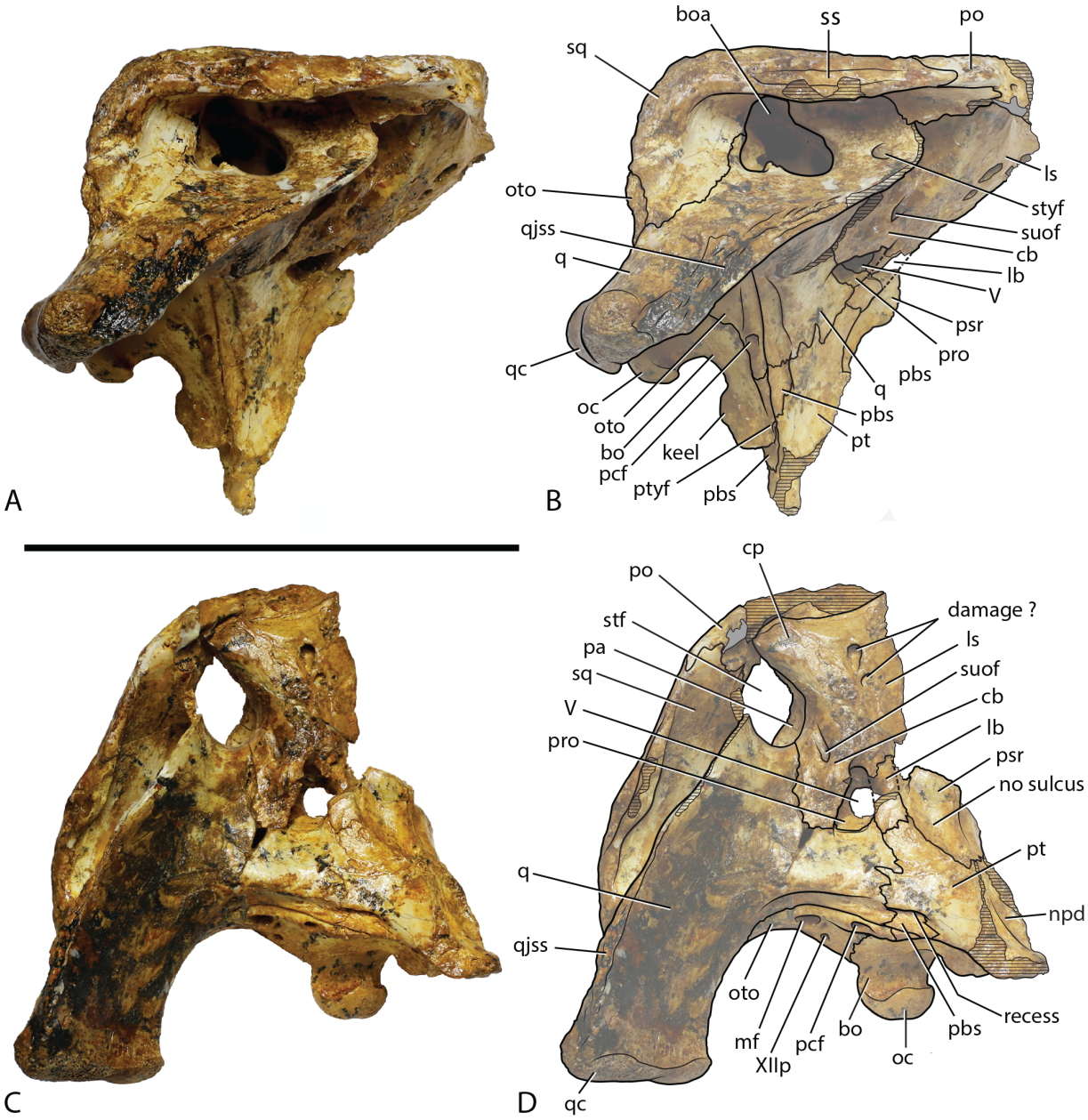

FIGURE 4. *Ultrastenos huberi*, QM F31075, White Hunter Cranial Form 1, posterior cranial fragment. A, B, right lateral view as a photograph (A), and as an annotated photograph with interpretive overlay (B). C, D, right ventrolateral view as a photograph (C), and an annotated photograph with interpretive overlay (D). Abbreviations: bo, basioccipital; boa, bony otic aperture; cb, caudal bridge of the laterosphenoid; cp, capitate process of the laterosphenoid; lb, lateral bridge of the laterosphenoid; ls, laterosphenoid; mf, metotic foramen; npd, posterior wall of the nasopharyngeal duct; oc, occipital condyle; oto, otoccipital; pa, parietal; pbs, parabasisphenoid; pcf, posterior carotid foramen; po, postorbital; pro, prootic; psr, base of parasphenoid rostrum; pt, pterygoid; ptyf, pharyngotympanic foramen; q, quadrate; qc, quadrate condyle; qjss, sutural surface for articulation with the quadratougal; sq, squamosal; ss, squamosal sulcus; stf, supratemporal fenestra; styf, subtympanic foramen; suof, supraorbital foramen; V, foramen for cranial nerve V (trigeminal foramen); XIIp, posterior foramen for cranial nerve XII (posterior hypoglossal foramen). Scale bar equals 50 mm.

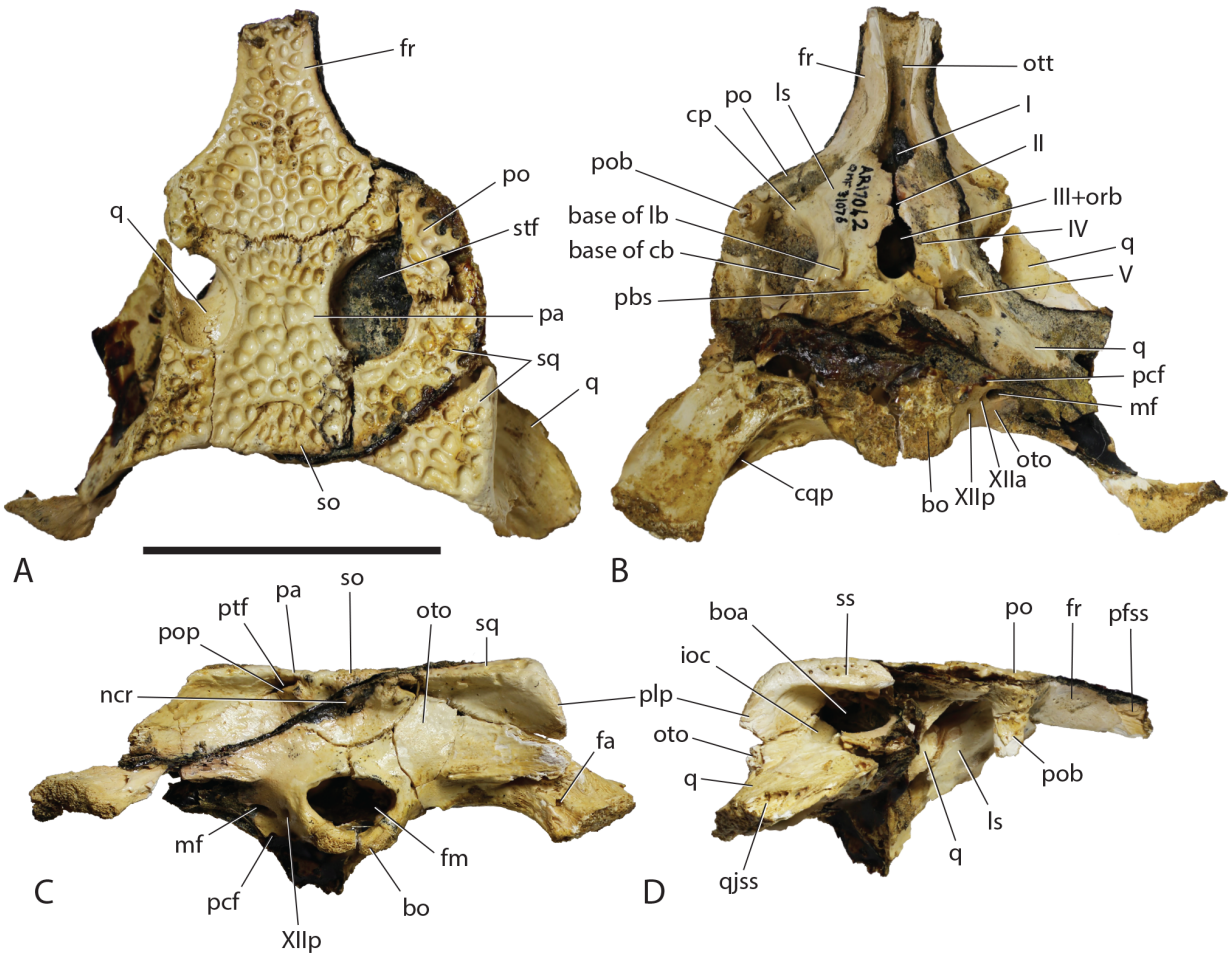

FIGURE 5. *Ultrastenos huberi* QM F31076, White Hunter Cranial Form 1, posterior cranial fragment. A, dorsal view. B, ventral view. C, occipital view. D, right lateral view. Abbreviations: bo, basioccipital; boa, bony otic aperture; cb, caudal bridge of the laterosphenoid; cp, capitate process of the laterosphenoid; cqp, cranioquadrate passage; fa, foramen aereum; fm, foramen magnum; fr, frontal; I, foramen for cranial nerve I (olfactory foramen); II, foramen for cranial nerve II (optic foramen); III+orb, common foramen for cranial nerve III (oculomotor nerve) and the orbital artery and vein; ioc, incisure of the cranioquadrate passage in the otic aperture; IV, foramen for cranial nerve IV (trochlear foramen); lb, lateral bridge of the laterosphenoid; ls, laterosphenoid; mf, metotic foramen; ncr, nuchal crest; oto, otoccipital; ott, olfactory tract trough; pa, parietal; parp, paroccipital process; pbs, parabasisphenoid; pcf, posterior carotid foramen; pfss, sutural surface for articulation with the prefrontal; plp, posterolateral process of the sqamosal; po, postorbital; pob, postorbital bar; pop, postoccipital process of the supraoccipital; ptf, posttemporal fenestra; q, quadrate; qjss, sutural surface for articulation with the quadratougal; so, supraoccipital; sq, squamosal; ss, squamosal sulcus; stf, supratemporal fenestra; V, foramen for cranial nerve V (trigeminal foramen); XIIa, anterior foramen for cranial nerve XII (anterior hypoglossal foramen); XIIp, posterior foramen for cranial nerve XII (posterior hypoglossal foramen). Scale bar equals 50 mm.

Stein et al. (2016b) noted that altirostral crocodylians, including *Mekosuchus* spp., possess a surangular with an elevated dorsal margin relative to that of the dentary, indicating that QM F42665 was not an altirostral form.

Stein et al. (2016b) also describe the retroarticular process of the mandible (Figure 2I) as relatively elongate compared to other mekosuchines and that although it was not as elongate as those of *Gavialis gangeticus* (Gmelin, 1789) or *Tomistoma schlegelii* (Müller, 1838), it does approach the proportion seen in the longirostrine *Crocodylus johnstoni* Krefft, 1873.

Lastly, Stein et al. (2016b) note that the preserved dentary teeth (the last four of the row) appear to be homodont which would be congruent

with, but not necessarily diagnostic of, homodonty of the entire tooth row. A high degree of homodonty is indeed significantly correlated with a slender elongate rostrum in regression analyses (Iijima, 2017; D'Amore et al., 2019).

Characteristics discordant with longirostry in QM F42665

Set against the features suggesting that QM F42665 had a slender longirostrine morphology are other morphological features that conflict with this interpretation (Table 1).

In his study of characters correlated with rostral shape, Iijima (2017) found the depth of the skull in posterior view, from the dorsal margin of the skull deck to the ventral margins of the pterygoid flanges (a measurement he called 'pterygoid flange depth') was significantly correlated with rostral shape, with deeper skulls correlating with the brevirostrine condition. Although Stein et al (2016b) suggested that the skull of QM F42665 was shallow, based on the shape and proportions of the lower jaw, the braincase fragment suggests otherwise. In posterior view, there is a dorsoventrally deep, transversely narrow basioccipital body extending ventral to the occipital condyle, and more significantly a dorsoventrally deep exposure of the parabasiphenoid and pterygoid ventral to the basioccipital (Figure 3C-D). These characters are associated with a large pterygoid flange depth and a brevirostrine skull (Iijima, 2017). Occipital proportions are even clearer in the more complete skull fragment QM F31075 ('WH cranial form 1') where the occiput has proportions that are closer to those of brevirostrine taxa than to slender longirostrine taxa (Figure 6A-C).

The teeth of longirostrine taxa are frequently described as 'needle-like' (e.g. Erickson et al., 2012) and indeed an average tooth shape that is highly caniniform is significantly correlated with longirostry when PCA analyses of tooth shape and rostral shape are regressed against one another (D'Amore et al., 2019). The posterior dentary teeth of QM F42665 do not fit this trend as they are apicodistally short, mesiodistally broad and close to equilateral, which is a recurrent tooth morphology in Crocodylia that is labelled 'molariform' (D'Amore et al., 2019). Molariform teeth of the form seen in QM F42665 are otherwise unknown in the slender longirostrine category.

Lastly, the relative size of the supratemporal fenestrae on the skull table argue against longirostry. Iijima (2017) found a significant positive correlation between the relative surface area of the supratemporal fenestra and longirostry. Rio and Mannion (2021) scored relative supratemporal fenestra size as a continuous character (character 10) in their cladistic analysis by using the ratio of the maximum anteroposterior length of the supratemporal fenestra to the anteroposterior length of the cranial table. While the holotype of *U. willisi* does not preserve the supratemporal fenestra, the left fenestra of the referred specimen QM F31076 is complete enough for measurement (Figure 5A-B). It yields a ratio of 0.386. This lies below the ratio scored for all members of the slender longirostrine category in their matrix (Rio and Mannion, 2021) with the sole exception of *C. intermedius* Graves, 1819 (0.357-0.465: Rio and Mannion, 2021, supplementary file 23). *Crocodylus intermedius* is one of the least specialised longirostrines and appears somewhat intermediate between the

TABLE 1. A summary of the arguments for and against slender longirostry in QM F42665 utilising the specimens referred to *'U. willisi'* in Stein et al. (2016), prior to the taxonomic revisions made in this paper.

Arguments for slender longirostry	Counterarguments	Arguments for brevirostry
Marked transverse constriction of the dentigerous portion of the mandible	Constriction is an artefact caused by a) damage to the mandible and b) articulation with a misaligned temporal fragment in the reconstructed skull	–
Proportionally shallow mandible indicates shallow skull correlated with slender longirostry	Uncrushed posterior cranial fragment QM F31075 has a proportionally deep occiput indicating cranial proportions closer to brevirostrine taxa.	–
Proportionally elongate retroarticular process	Relative length of retroarticular process is ambiguous	–
–	–	Proportionally small supratemporal fenestrae.
–	–	Blunt, molariform, posterior dentary teeth.

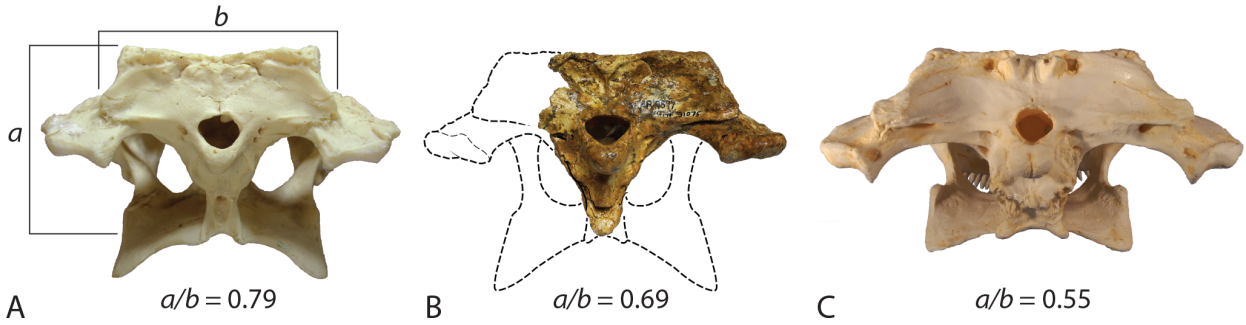

FIGURE 6. Comparison of the occipital proportions of various crocodylians. A: *Osteolaemus tetraspis* NTM unregistered cast, a brevirostrine form. B: *Ultrastenos huberi*, QM F31075. C. *Tomistoma schlegelii*, NTM P3142 (cast), a slender longirostrine form. Images are not to scale.

fully longirostrine species and more generalist mesorostrine species in other measures (Iijima, 2017, figure 3). So the proportion seen in QM F31076 is unusually low for the slender longirostrine category, but it is typical for basal mekosuchines (e.g., *Kambara implexidens* Salisbury and Willis, 1996: 0.399-0.415 and *Australosuchus clarkae* Willis and Molnar, 1991a: 0.340-0.482; Rio and Mannion, 2021, supplementary file 23) with generalist, mesorostrine rostra.

MATERIALS AND METHODS

This study is based on a first hand examination of all the material referred to either *U. willisi*, 'WH cranial form 1' or *'B.' huberi* (listed in systematic paleontology) by one or both of the authors. All of this material is held and curated by the Queensland Museum, Brisbane, Australia. Measurements were taken to the nearest tenth of a millimetre using a set of hand-held 150 mm digital calipers. Images were taken with a digital SLR camera and final images were created using 'focus stacking' in digital imaging software.

Institutional Abbreviations. NTM, Museum and Art Gallery of the Northern Territory, Darwin and Alice Springs, Northern Territory, Australia; QM, Queensland Museum, Brisbane, Queensland, Australia; UCMP, Museum of Paleontology, University of California, Berkeley, California, USA.

TAXONOMY

Does WH Cranial Form 1 Belong to *'Baru' huberi*?

At the heart of the revised taxonomy, and morphological reconstruction, of *Ultrastenos* presented here, lies the systematic position of the specimens Willis (1997) called 'WH cranial form 1'. It is argued that not only does 'WH cranial form 1' belong to *'B.' huberi* but QM F31076 is the posterior end of the same individual skull as QM F31060, the holotype rostrum of *'B.' huberi* (Figure 7). Evidence for this association comes from preservation style, matching size, near matching broken surfaces, shared apomorphic ornamentation, lack of alternative rostra and braincases at the site, and a related taxon from the Middle Miocene of Bullock Creek combining characters of each.

Similar preservation. Both QM F31060 and QM F31076 were collected from White Hunter site. The preservational style at White Hunter site is quite variable between specimens. The colour of the bone surface varies from a rich, orangey-brown (e.g., QM F31075) through paler creamy brown (e.g., QM F31062) to whitish cream (QM F31076). The degree of speckling from manganese mineralisations on the surface also varies between specimens from moderately speckled with heavy patches (e.g., QM F31075) to almost none (e.g., QM F31076). Both QM F31060 and QM F31076 share the whitish cream colour with almost no manganese speckles. These two specimens also display a moderate degree of postmortem dorsoventral flattening not observed in QM F31075.

Matching size. The specimens QM F31060 and QM F31076 are both of similar size. This is especially evident at the anterior end of the interorbital bridge where the two specimens approach most closely without any mismatch in size that indicates they are plausibly parts of the same skull.

Near matching of broken surfaces. Unfortunately the two pieces lack a direct connection where two broken surfaces join, uniting the skull into one piece, however, the posterior interorbital region of QM F31060 closely approaches and parallels the anterior end of the interorbital bar of QM

FIGURE 7. *Ultrastenos huberi*, QM F31060 (holotype, maxillary rostrum) and QM F31076 (posterior cranial table) placed in approximate life position, relative to each other, in dorsal view. Scale bar equals 50 mm.

F31076. Furthermore these broken surfaces are stained dark grey/black indicating that the breaks were natural erosional surfaces. We suggest that the rostrum and posterior skull were severed by a fissure in the limestone that became weathered and eroded prior to collection. In this way, the two pieces came to be collected in two non-joining blocks, which would explain how the two parts of the skull came to be registered separately and the association lost.

The evidence above suggests that QM F31060 and QM F31076 are parts of the same individual. While this is not conclusive, the following evidence indicates that nevertheless the two specimens belong to the same species:

Distinctive shared ornamentation. Ornamentation of the dermal bones is not frequently employed in the systematics of Crocodylia, and it can vary considerably from area to area on the same specimen. Nevertheless, systematic variation is apparent when comparing homologous areas and similar ontogenetic stages. The ornamentation present on the skull table of QM F31076 is distinguishable from other crocodylian species present in the White Hunter Local Fauna, and it is also present on the median dorsal region of QM F31060, especially the prefrontals and lacrimals. This ornamentation consists of rounded, subcircular pits of regular size, separated by ridges of even height (Figure 8D-F). The ornamentation seen on comparable parts of *B. wickeni* differ in having pits of less regular size and frequently irregular shape, separated by ridges of varying height (Figure 8A-C). The ornament at the centre of the frontal of *M. whitehunterensis* (QM F31052) is similar to the ornament on QM F31060 and QM F31076 but does differ in having less regularly-sized pits. This is, however, not relevant as the known parts of *M. whitehunterensis* can be easily distinguished from both QM F31060 and QM F31076 on other grounds. The broad interorbital distance on the frontal of *M. whitehunterensis* is very different from the narrow interorbital distance in QM F31076, while its broad, blunt-ended anterior process differs from the acute anterior tip of the frontal seen in QM F31060. The ornament of *Q. meboldi* is difficult to characterise because the referred specimens do not include parts of the skull table, posterior mandible, or median dorsal rostrum where taxonomically distinct dermal ornamentation reaches its full development. Nevertheless, these parts of the closely related *Q. timara* Megirian, 1994, are known and reveal a rather different style of ornamentation (Figure 9A, B) to 'WH cranial form 1'. In *Q. timara* the dorsal surfaces of the squamosals, parietal, frontal, postorbital, and posterior surangular bear angular, irregularly polygonal pits separated by broad ridges. It should be noted here that these parts of *Q. timara* are currently undescribed but can be referred to the genus *Quinkana* because they match fragments from the Ongeva Local Fauna, where the only known crocodylian is a species of *Quinkana* (A.M. Yates, pers. obs. of multiple specimens at NTM, in 2022). In this case, the deposit is interpreted as monospecific because all of the shed crocodylian teeth are of the labio-lingually compressed ziphodont type, attributable to *Quinkana*. Furthermore, the squamosals

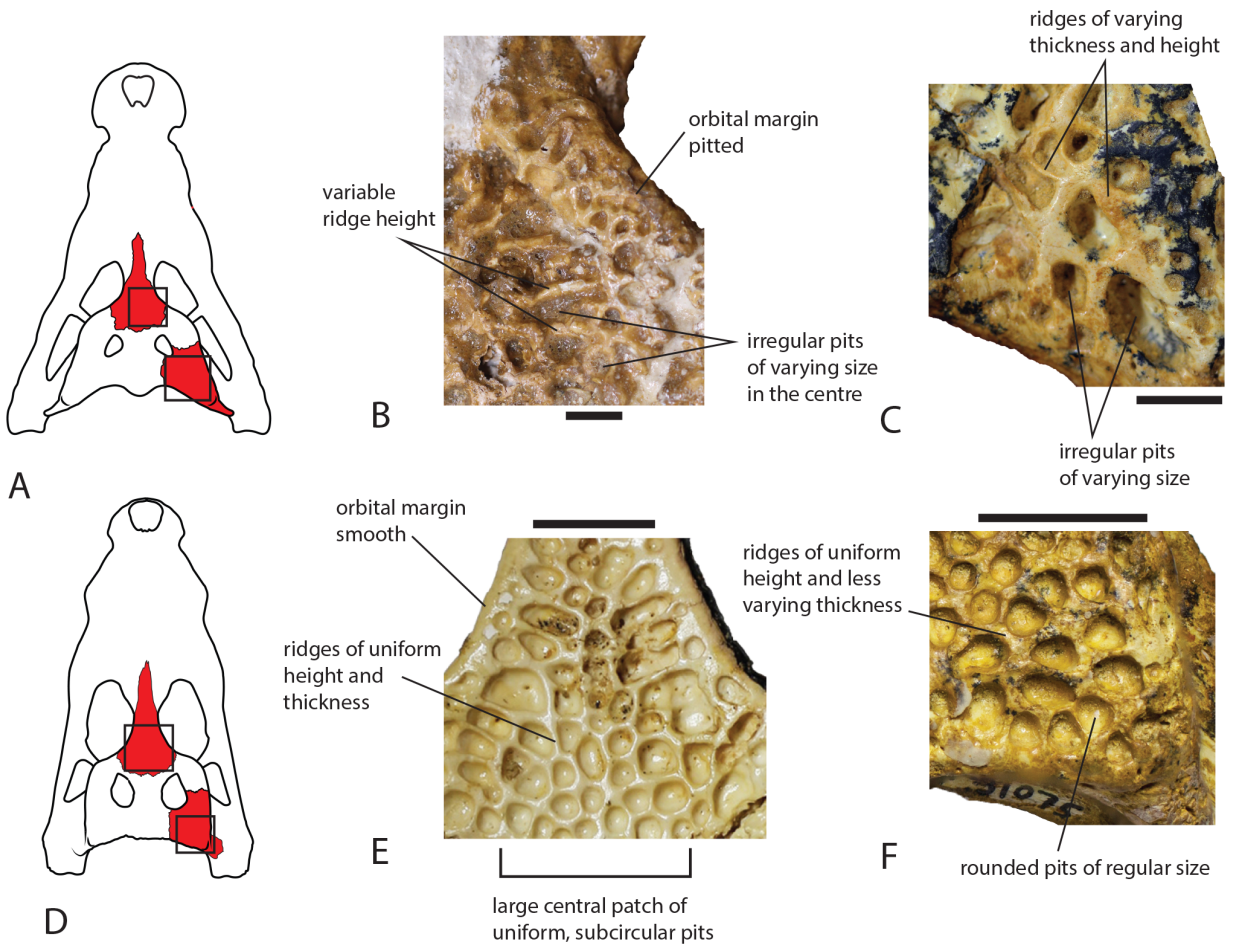

FIGURE 8. Dermal bone ornamentation of *Baru wickeni* and *Ultrastenos huberi* compared. A: Explanatory drawing of the skull of *Baru wickeni* in dorsal view with frontal and right squamosal marked in red and the areas shown in (B) and (C) marked by boxes. B: *Baru wickeni* (NTM P91171-1), frontal in dorsal view showing the ornamentation. C: *Baru wickeni* (NTM P902-4), right squamosal in dorsal view showing the ornamentation. D: Explanatory drawing of the skull of *Ultrastenos huberi* in dorsal view with frontal and right squamosal marked in red and the areas shown in (E) and (F) marked by boxes. E: *Ultrastenos huberi* (QM F F31076), frontal in dorsal view showing the ornamentation. F: *Ultrastenos huberi* (QM F F31075), right squamosal in dorsal view showing the ornamentation. Scale bars in (B, C, E, F) equal 10 mm. (A, D) are not to scale.

referred to *Quinkana timara* share a suite of traits with the squamosal of *Quinkana* sp. from the Ongeva Local Fauna, including dermal ornamentation extending onto the floor of the lateral squamosal sulcus, narrowing of the lateral ventral ridge that bounds the meatal chamber and the distinctive dermal ornamentation described above. Full descriptions of both the Bullock Creek and Ongeva *Quinkana* specimens are presently in preparation.

The distinctive ornamentation that is attributed to *Quinkana* here, is also seen on the parietal of a cranial table fragment (QM F31079) from the White Hunter Local Fauna (Figure 9C, D). Willis (1997) designated this specimen 'White Hunter cranial form 2'. 'WH cranial form 2' also shares an anteroposteriorly elongate, transversely narrow supratemporal fenestra with *Q. timara* and can be referred to *Q. meboldi* with a reasonable degree of confidence. Given these differences in ornamentation, especially of the skull table, that the different mekosuchines of the White Hunter Local Fauna display, the presence of very similar ornamentation on parts of both QM F31076 and QM F31060 is good evidence that they belong to the same species.

Lack of alternative rostra and posterior crania. If we were to reject the hypothesis that *'Baru' huberi* and 'WH cranial form 1' are parts of the same species, then we are left with the necessary alternative that there must be a different rostral

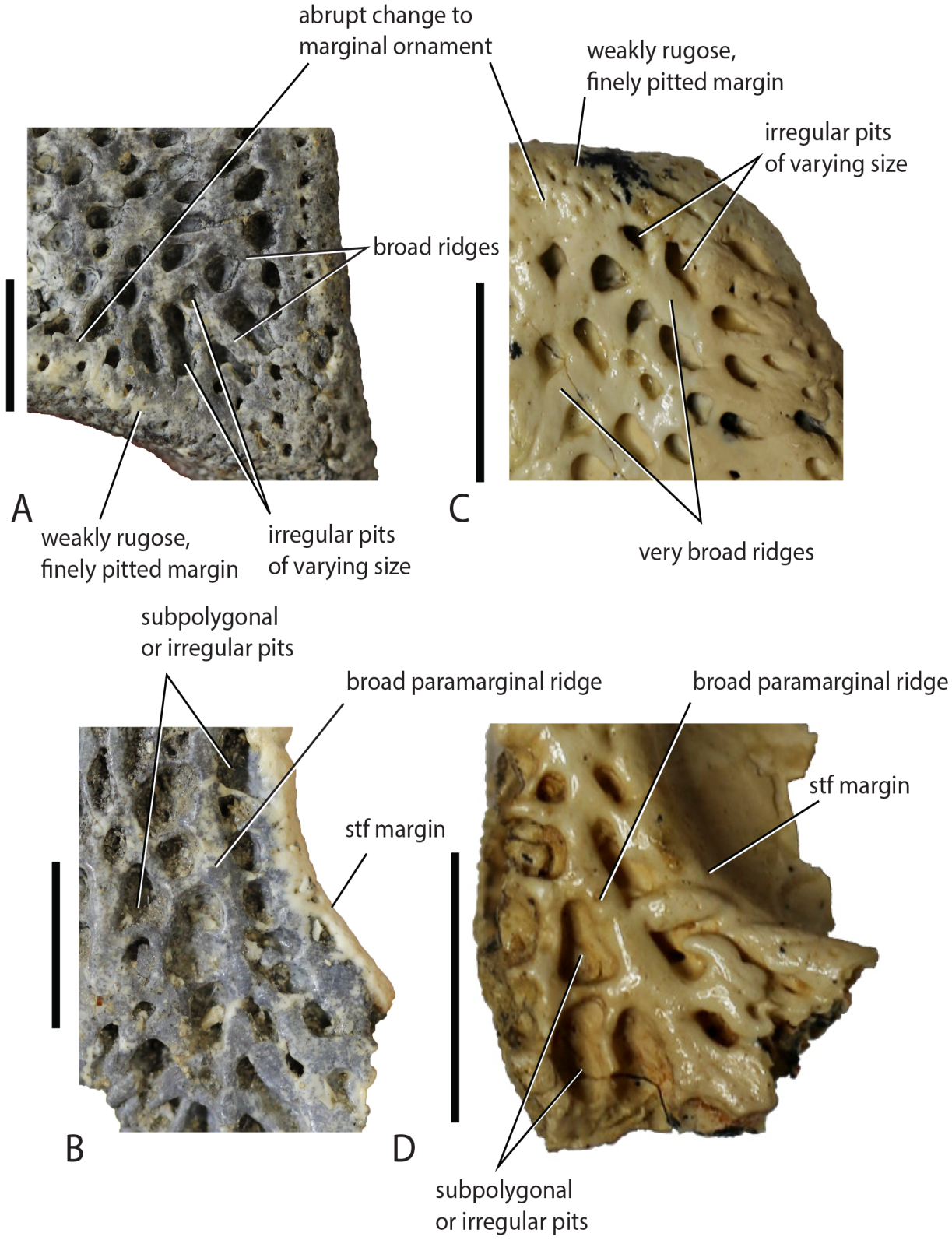

FIGURE 9. Comparison of *Quinkana timara* to White Hunter Cranial Form 2, QM F31079, here referred to *Q. meboldi* Willis. A: *Q. timara* (NTM P8695-114), right squamosal. B: *Q. timara* (NTM P9464-177), parietal margin of the right supratemporal fenestra. C, D: *Q. meboldi* (QM F31079), posterior cranial fragment. B, right postorbital. C, parietal margin of the right supratemporal fenestra. Scale bars equal 10 mm.

form that belongs to 'WH cranial form 1' and another posterior skull form that belongs to *'B.' huberi* that are, as yet, unknown. Taking *'B.' huberi* first, there is a second cranial form ('WH cranial form 2') that could conceivably represent the missing posterior cranial region of this species, but as argued above it is evident that 'WH cranial form 2' belongs to *Q. meboldi*. This also rules out *Q. meboldi* as a potential rostrum to go with 'WH cranial form 1'. As we have argued above, *M. whitehunterensis* can be distinguished from both *'B.' huberi* and 'WH cranial form 1' so cannot be the missing rostrum or posterior cranium of either. The posterior skull of *B. wickeni* is also known (Yates, 2017) and demonstrates a host of systematically significant differences to 'WH cranial form 1' (see below) thus ruling this species out as a candidate rostrum of 'cranial form 1'. We are left with the conclusion that if the rostrum of *'B.' huberi* does not belong with 'WH cranial form 1' then the rostrum of 'WH cranial form 1' is entirely unknown. By itself this is not an especially unusual situation but it is worth noting that *'B.' huberi* is the most abundant crocodylian in the White Hunter Local Fauna, with at least four rostral fragments and three anterior mandibular fragments referrable to it, while four of the six known posterior skull fragments are 'WH cranial form 1' (tallied from Willis, 1997). It is certainly not impossible for biased sampling to have failed to produce any posterior cranial parts of *'B.' huberi* or rostral pieces of 'WH cranial form 1' but it is more plausible that the two represent a single, locally common species.

Related species from the Bullock Creek Local Fauna. Included among the crocodylian remains recovered from the Middle Miocene Bullock Creek Local Fauna of the Northern Territory are a residue of specimens that cannot be referred to the named crocodylians from that fauna, namely *B. darrowi* Willis et al., 1990, *Q. timara*, and *H. camfieldensis*. Lee and Yates (2018) informally labelled these the 'Bullock Creek taxon'. The 'Bullock Creek taxon' displays the same kind of dermal ornamentation seen in WH cranial form 1 (QM F31076 and QM F31060) and include rostral and posterior skull pieces that share apomorphic characters with both the rostral specimens referred to *'B.' huberi* and the posterior cranial specimens referred to 'WH cranial form 1' (Figure 9). We will not exhaustively document these fossils, as another paper in preparation will describe and name this new species. However, a few salient specimens and anatomical features will be highlighted to illustrate their relevance to the topic of this paper. NTM P87115-3 is a posterior cranial fragment that shares rounded posterior, medial, and lateral margins of the supratemporal fenestra and a steeply descending subdermal component of the posterolateral process of the squamosal with 'WH cranial form 1' (Figure 10A, B). A maxilla (NTM P9660) shares an enlarged anterior neurovascular foramen medial to the first alveolus, a transverse premaxilla-maxilla suture anterior to the level of the first maxillary alveolus and a medial ridge bordering the lateral premaxilla-maxilla notch with *'Baru' huberi* (Figure 10C). Once again, the rostral parts do not directly join the posterior cranial parts, and the unity of the hypodigm must be inferred from other evidence. Nevertheless, the repeated co-occurrence of similar parts mutually reinforces the hypothesis that the 'Bullock Creek taxon' represents dissociated parts of a single taxon while *U. willisi* and *B. huberi* represent the dissociated parts of a related (but specifically distinct) taxon. However, in this case of the 'Bullock Creek taxon' there is a largely complete mandibular ramus (NTM P895-15; Figure 10D), which combines a postdentary region directly with a dentary of brevirostrine proportions. The postdentary region of NTM P895-15 shares derived character traits with the holotype of *'U. willisi'* including a reduced external mandibular fenestra and a posterior dorsal process of the dentary that extends beyond the posterior corner of the external mandibular fenestra.

This mandible demonstrates conclusively that the *Ultrastenos*-like components of the 'Bullock Creek taxon' belong to a brevirostrine taxon and that, by extension, the very similar and closely related posterior cranial pieces referred to *U. willisi* almost certainly do as well.

Systematic Position of QM F31075

A short discussion regarding the identity of QM F31075 needs to be included here. QM F31075 was one of the two specimens from White Hunter Site included in 'cranial form 1' by Willis (1997) and referred to *U. willisi* by Stein et al. (2016b). Yates (2017) disagreed and thought that this specimen in particular (but not QM F31076, the second specimen referred to 'WH cranial form 1') was in fact an immature individual of *B. wickeni*. Evidence for this came from the recognition that QM F31075 and NTM P91171-1, a skull that uncontroversially is referred to *B. wickeni* (Yates, 2017), shared two derived characters: the broad exposure of an occipitally-facing surface of the quadrate ventrolateral to the otoccipital and dorso-

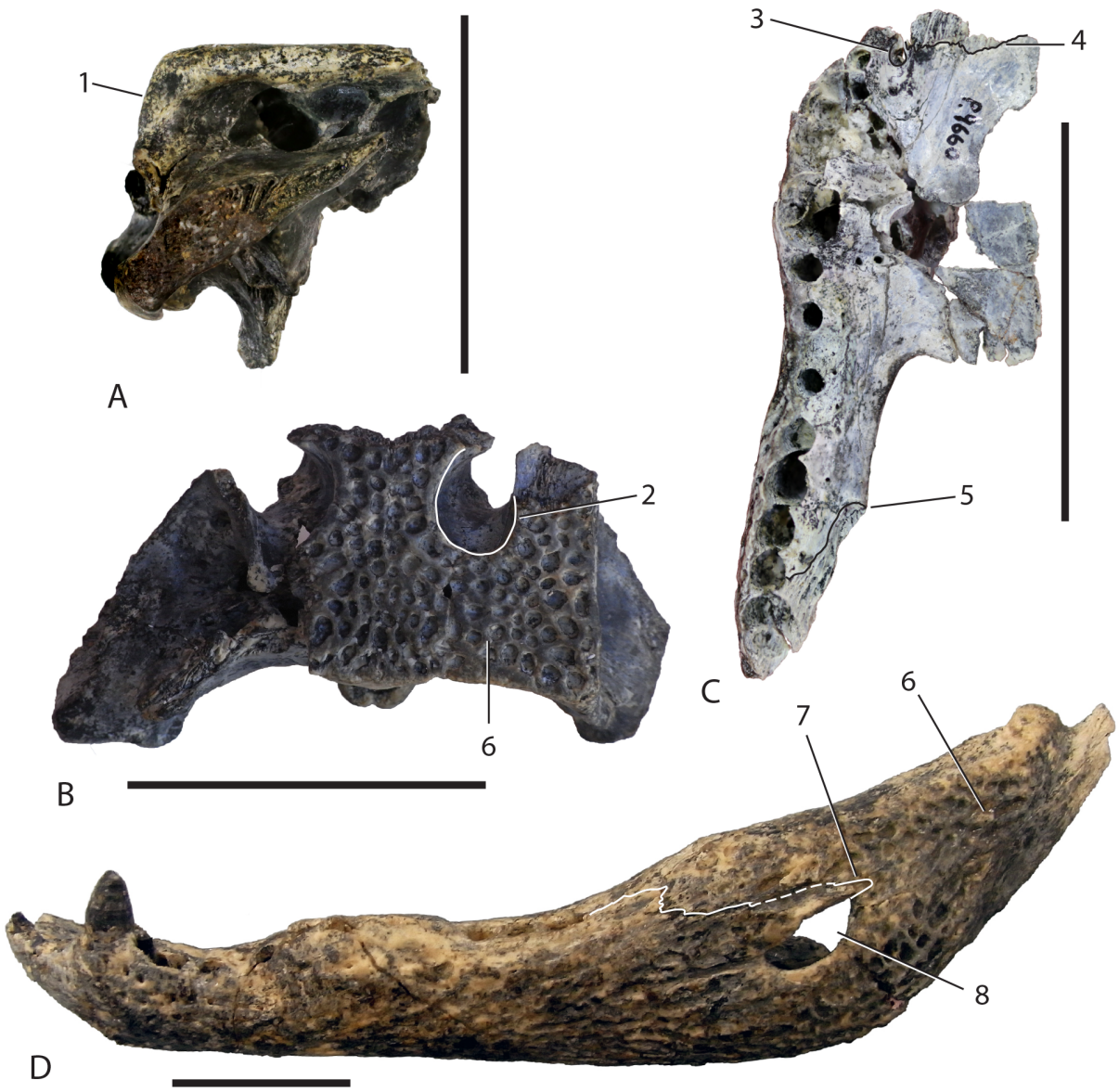

FIGURE 10. *Ultrastenos* sp. "Bullock Creek Taxon", isolated specimens from the Middle Miocene, Bullock Creek Local Fauna, Northern Territory. A, B: NTM P87115-3, posterior cranial fragment. A, right lateral view. B dorsal view. C: NTM P9660, right maxilla in ventral view. D: NTM P895-15, left mandibular ramus in lateral view. Derived character states shared with *U. huberi* Willis: 1, posterolateral process of the squamosal descends at a steep angle (74º); 2, medial, posterior and lateral margins of the supratemporal fenestra rounded and curve gradually into one another; 3, enlarged anterior maxillary foramen; 4, transverse palatal premaxillomaxillary suture lying anterior to the level of the first maxillary alveolus; 5, absence of a posterior lamina of the maxilla separating the anterior tip of the ectopterygoid from the margin of the suborbital fenestra; 6, dermal ornament consisting of regular, subcircular pits separated by walls of even height; 7, posterior extent of the dentary posterior to the posterior margin of the external mandibular fenestra; 8, length of the reduced external mandibular fenestra is less than 25% of the distance between the dentary toothrow and the anterior margin of the mandibular glenoid. Scale bars equal 50 mm.

ventrally deep exposure of the parabasisphenoid ventral to the basioccipital.

Differences between QM F31075 and larger specimens of *B. wickeni* were dismissed as ontogenetic variation (Yates 2017). However, the subsequent description of *B. iylwenpeny* Yates et al., 2023 from Alcoota, including juvenile specimens, indicates that these character differences are not due to ontogeny. Perhaps the most striking difference between QM F31075 and *B. wickeni* is the angle that the dorsal profile of the posterolateral process of the squamosal makes with the skull table in lateral view (Figure 11A, B). In QM F31075 this angle is steep, and approaches a right angle (Figure 11A) whereas in *Baru*, whether adult or juvenile, the posterolateral process slopes shallowly towards the dorsolateral corner of the paroccipital process (Figure 11B-D). Similarly the presence of a single well-developed longitudinal sulcus on the lateral surface of the squamosal in QM F31075 (Figure 11A) differs from the flattened lateral surface of the squamosal in both adult *B. wickeni* and juvenile *B. iylwenpeny* that are crossed by one or two short, discontinuous, narrow sulci (Figure 11B-D). Another difference is the posteriorly rounded supratemporal fenestrae of QM F31075 differ from the 'D'-shaped fenestrae with a straight medial margin seen in adult *B. wickeni* and juvenile *B. iylwenpeny*. Lastly QM F31075 possesses the same kind of dermal ornamentation on the skull table (Figure 8F) that is seen in other specimens of 'WH cranial form 1', best represented by QM F31076. From these observations we conclude that QM F31075 is not a juvenile specimen of *B. wickeni* (contra Yates, 2017), and it does indeed belong to the same taxon as 'cranial form 1' as other authors have concluded (Willis, 1997; Stein et al., 2016b).

Synonymy of *Ultrastenos willisi* and '*Baru*' *huberi*

The holotypes of *Ultrastenos willisi* and *'B.' huberi* lack overlapping parts so that the subjective synonymy of these two species rests almost entirely upon referred specimens, namely those cranial fragments labelled 'WH cranial form 1'. If

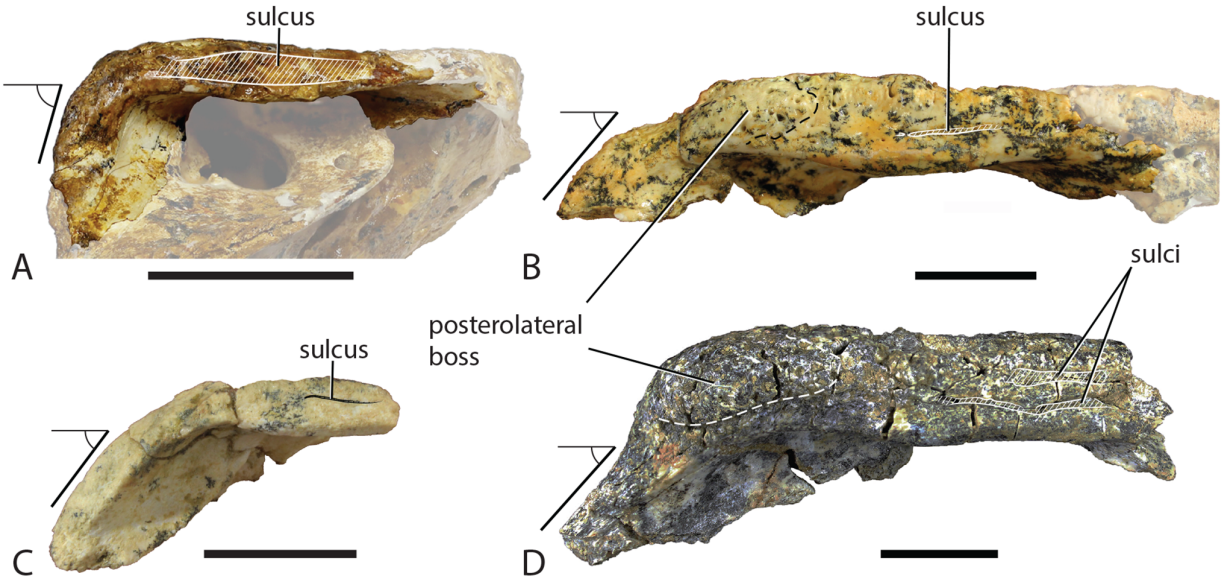

FIGURE 11. Comparison of the squamosal in right lateral view of *Ultrastenos huberi* with various species of *Baru*, showing the angle of descent of the posterolateral process and sculptural elements of the lateral surface. A: *Ultrastenos huberi*, QM F31075. Note that the lateral squamosal sulcus is both broad and extensive and the posterolateral process descends at a steep angle. B: *Baru wickeni*, NTM P9464-10 (image reversed for comparison). Note that the lateral surface is largely flat with a short, narrow sulcus and the posterolateral process descends at a shallow angle. C: Juvenile *Baru iylwenpeny* (NTM P6478). Note the flat lateral surface with a short, narrow sulcus and the shallow angle of descent. D: Adult *Baru iylwenpeny* (NTM P6515) Note the flat lateral surface with a short, narrow sulcus and the shallow angle of descent shared with other *Baru* specimens. Note also the presence of a posterolateral boss shared with (B) but not (C). Dashed lines demarcate each posterolateral boss. Hatched areas demarcate lateral sulci. Scale bars equal 20 mm.

we accept the case made above that 'WH cranial form 1' represents the posterior part of the skull of *'B.' huberi* and if we also accept that 'cranial form 1' is the same species as *U. willisi* then the latter becomes a junior synonym of the former. Therefore, it is important to determine if 'WH cranial form 1' can be securely referred to the same taxon as *U. willisi* as Stein et al. (2016) did. No unambiguous autapomorphies can be identified but 'WH cranial form 1' does share a unique combination of derived characters with the holotype of *U. willisi* that allow them to be distinguished from all other crocodylian species. Some of these characters have the potential to optimize as autapomorphies once the character state distributions and phylogenetic relationships within Mekosuchinae become better understood. These derived characters states are: short, steeply descending posterolateral process of the squamosal (Figure 12B, F); short quadrate body with the distance between the distal tip of the paroccipital process and the dorsal margin of the quadrate condyle less than the transverse width of the quadrate condyle (Figure 12A, E); the parabasisphenoid-pterygoid suture on the lateral wall of the braincase is recessed within a sulcus that parallels the posterolateral margin of the braincase (Figure 12C, G); a highly reduced, to absent contribution of the otoccipital to the synovial surface of the occipital condyle (Figure 12D, H); an enlarged ventral sagittal keel on the basioccipital plate that is prominent in lateral view (Figure 12C, G); and a dorsoventrally deep, sheet-like exposure of the parabasisphenoid ventral to the median pharyngeal tube foramen (Figure 12D, H). On the basis of this unique combination of character states 'WH cranial form 1' and the holotype of *U. willisi* are considered to represent the same species and for which *'B.' huberi* is the oldest available name.

Validity of *Ultrastenos*

'Baru' huberi displays a number of characteristics that differ markedly from other species of *Baru*, especially once the posterior skull characters afforded by QM F31075, F31076, and F42665 are taken into consideration. These include: an anteroventrally tilted opening of the external naris which contributes to a shallower anterior profile of the premaxilla in lateral view; a platyrostral rostrum with a decreased degree of ventral undulation ('festooning') of the maxillary tooth row; a narrow Interorbital bridge with the dorsomedial margins of the orbit flush with the dorsal surface of the skull roof; a single well-developed lateral squamosal sulcus; a steeply descending posterolateral process of the squamosal; the absence of a sulcus on the anterior surface of the braincase, immediately lateral to the base of the parabasisphenoid rostrum; a reduced external mandibular fenestra less than 25% of the length between the mandibular glenoid and the posterior end of the dentary tooth row; and an anterior tip of the splenial that lies ventral to the Meckelian sulcus.

Only Lee and Yates (2018) have included both the 'Bullock Creek taxon' and *U. huberi* (including data from both the rostral and posterior cranial regions) in a phylogenetic analysis. They found that the two species formed a clade that shared a more recent common ancestor with other mekosuchine genera including *Volia, Mekosuchus, Trilophosuchus,* and *Quinkana* than it did with other *Baru*, including the type species, *B. darrowi*. Ristevski et al. (2023) also included *U. huberi* (as *'Baru' huberi*) in a phylogenetic analysis (but did not include the 'Bullock Creek taxon'). They also scored *U. huberi* for the full compliment of available anatomical data from both the rostrum and the posterior cranium. They too, found that *U. huberi* shared a more recent common ancestor with *Volia, Mekosuchus,* and *Trilophosuchus* (but not *Quinkana*) than with *Baru*, in all iterations of their analysis (Figure 13). Thus, multiple, independent analyses have found that *Ultrastenos* is not a synonym of, or even a sister taxon to, *Baru*. With the inclusion of the 'Bullock Creek taxon' it is revealed to be a lineage that persisted from at least the Late Oligocene to the Middle Miocene (longer if UCMP 70939, from the late Miocene of Alcoota also belongs to this lineage) alongside the altirostral macropredators that are true *Baru*. Under these circumstances a separate genus name is warranted and *Ultrastenos* Stein et al., 2016b, is the oldest, indeed only, available name.

SYSTEMATIC PALAEONTOLOGY

CROCODYLIA Gmelin, 1789
MEKOSUCHINAE (Balouet and Buffetaut, 1987)
MEKOSUCHINI (Balouet and Buffetaut, 1987), sensu Salisbury and Willis, 1996
ULTRASTENOS Stein, Hand, and Archer, 2016b

Type species. *Ultrastenos willisi* Stein, Hand, and Archer, 2016b, junior subjective synonym of *Baru huberi* Willis, 1997.

Diagnosis. Mekosuchines with the following apomorphic characters: lateral notch for the occlusion of the fourth dentary tooth at the premaxilla-maxilla suture bordered laterally and medially by sharp ridges; palatal premaxilla-maxilla suture anterior to

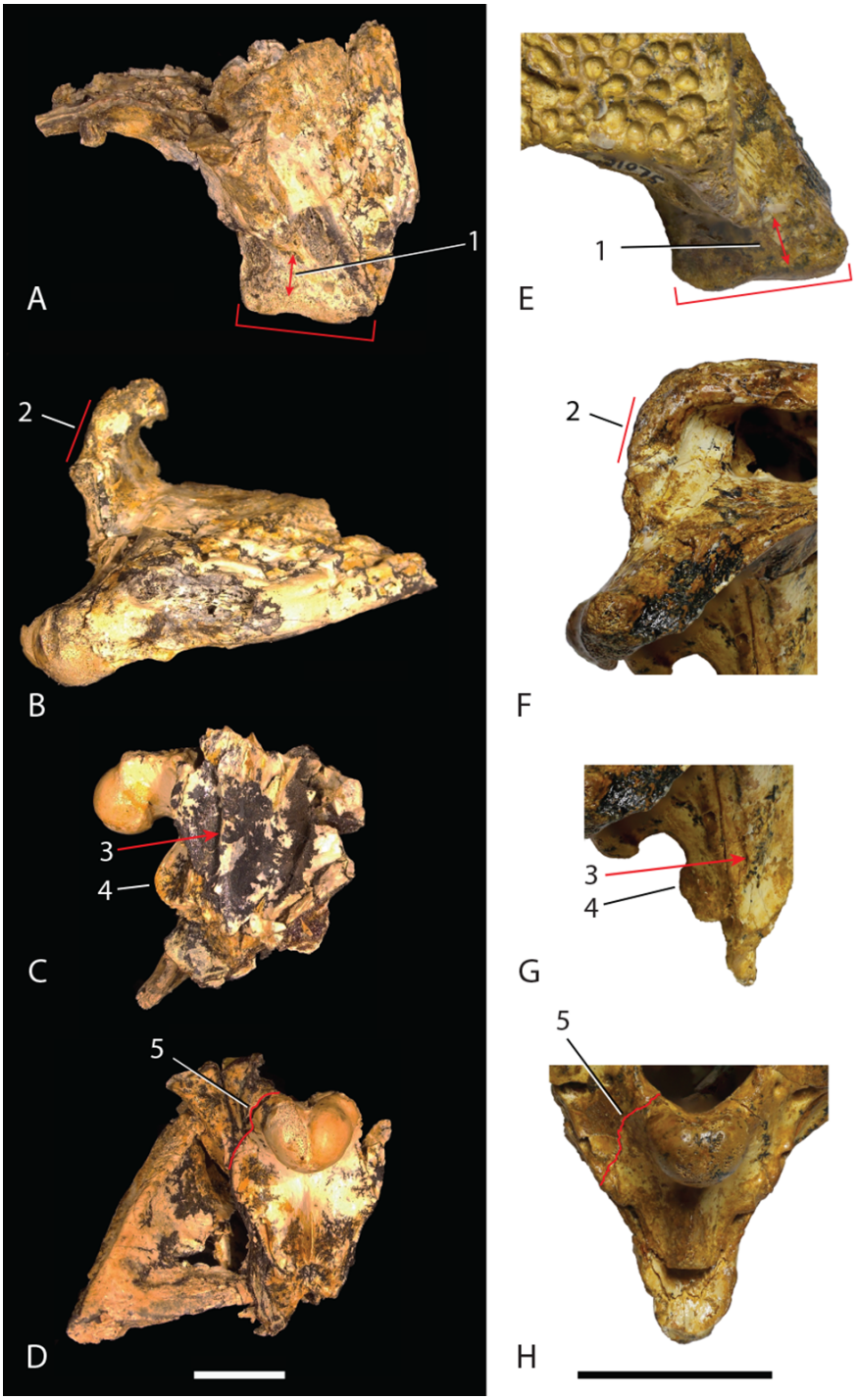

FIGURE 12. *Ultrastenos huberi* , shared derived character states. A-D: QM F42665, holotype of *Ultrastenos willisi*. A, B, Right temporal fragment in dorsal view (A) and lateral view (B). C, D, ventral portion of braincase (with attached, displaced fragment of right pterygoid) in right lateral view (C) and occipital view (D). E-H: QM F31075, 'WH Cranial Form 1'. E, F, right temporal region in dorsal view (E) and lateral view (F). G, H, ventral portion of braincase in right lateral view (G) and occipital view (H). Numbered character states: 1, distance from the ventrolateral tip of the paroccipital process to the dorsal margin of the quadrate condyle is less than the transverse width of the quadrate condyle (shown by rectangular bracket); 2, short posterolateral process of the squamosal descends at an angle steeper than 65º; 3, parabasisphenoid-pterygoid suture recessed within a sulcus; 4, enlarged sagittal, ventral keel of the basioccipital prominent in lateral view; 5, otoccipital-basioccipital suture (marked with red line) fails to cross the synovial surface of the occipital condyle. Scale bars equal 20 mm.

the first maxillary alveolus (convergent in some non-mekosuchines); enlarged neurovascular foramen adjacent to the first maxillary alveolus (convergent with *Q. timara* Megirian, 1994); supratemporal fenestrae roughly tear drop-shaped with rounded posterior margins and an acuminate anterior end; short, steeply descending posterolateral process of the squamosal (convergent in *Volia athollandersoni* Molnar et al., 2002); short quadrate body with the distance between the distal tip of the paroccipital process and the dorsal margin of the quadrate condyle less than the transverse width of the quadrate condyle (reversal to a non-mekosuchine condition); a highly reduced, to absent contribution of the otoccipital to the synovial surface of the occipital condyle; hypertrophied sagittal keel on the basioccipital plate ventral to the occipital condyle that is prominent in lateral view; recessed parabasisphenoid-pterygoid suture on lateral braincase wall that is hidden in lateral view (convergent with *B. darrowi*); dorsoventrally deep exposure of the parabasisphenoid and pterygoids ventral to the medial pharyngeal tube foramen (convergent with *B. wickeni* and many non-mekosuchines); posterodorsal process of the dentary terminates posterior to the posterior margin of the external mandibular fenestra; absence of lateral eversion of the ridges bordering the ornamented lateral surfaces of the surangular and angular (reversal to a non-mekosuchin condition).

In addition to these autapomorphies, *Ultrastenos* can be distinguished from other contemporary mekosuchine species by distinctive dermal ornamentation of the skull table, interorbital and central rostral regions of the skull and posterior region of the mandible which consists of regular sized, subcircular pits separated by level ridges.

Ultrastenos huberi (Willis, 1997) comb. nov.
Figures 1-8, 11-20, 22, 23

1997 *Baru huberi* Willis, p. 429, figures 10-11.

1997 'Cranial Form 1' Willis, p.435, figures 20-22.

2016 *Ultrastenos willisi* Stein, Hand, and Archer, p. e1179041-2, figures 1-4.

2017 *Baru wickeni*: Yates, p. e3458-30, figure 16e [partim].

Holotype. QM F31060, fragmentary rostrum.

Paratypes. QM F31061, right premaxilla and incomplete right maxilla; QM F31062, right premaxilla (herein removed from the hyodigm of *U. huberi*); QM F31063, right maxillary fragment (herein removed from the hypodigm of *U. huberi*); QM F31064, right maxillary fragment; QM F31065, maxillary fragment; QM F31066, maxillary fragment; QM F31067, dentary; QM F31068, left dentary; QM F31069, conjoined dentary pair with attached splenials.

Type locality and horizon. White Hunter Site, Riversleigh World Heritage Area, Queensland. Unnamed fluvio-lacustrine unit, Riversleigh Faunal Zone A, Late Oligocene.

Referred material. QM F31075, posterior skull fragment; QM F31076, incomplete postorbital region of skull; QM F31077, skull fragment; QM F31078, isolated parietal; QM F42665 (holotype of *Ultrastenos willisi*), fragmentary posterior skull and mandible; QM F42669, left atlantal neural arch (this specimen and all following specimens are paratypes of *Ultrastenos willisi*); QM F42668, atlantal intercentrum; QM F42670, caudal vertebrae series; QM F42672, osteoderms; QM F42673, metatarsal; QM F42667, right coracoid; QM F42666, right tibia. QM F61096, mandible, missing both postdentary areas; QM F61097, incomplete orbital region of the skull and left pterygoid.

Localities and horizons. Type locality (QM F31060, QM F31061, QM F31064, QM F31065, QM F31066, QM F31067, QM F31068, QM F31069, QM F31075, QM F31076, QM F31077, QM F31078, QM F61096, QM F61097); Low Lion Site (QM F42665, QM F42669, QM F42668, QM F42670, QM F42672, QM F42673, QM F42667, QM F42666). Both sites from un-named fluvio-lacustrine units of Riversleigh Faunal Zone A, Late Oligocene.

Diagnosis. As for the genus until new species are described.

Description

General features of the skull. Several of the more informative specimens of *U. huberi* have been described in either Willis (1997) or Stein et al. (2016b), so the description here is focused largely upon listing character states that have been used in cladistic analyses of crocodylian relationships.

The holotype of *'B.' huberi* has an estimated skull length of 200 mm and a width of 110 mm (Figure 7), although QM F42665 is distinctly larger, with a reconstructed posterior width of approximately 180 mm, which would indicate a skull length of about 350 mm. If the reconstruction presented here (Figure 14A-D) is accurate then it is a brevirostrine form with the rostrum occupying 48% of the total skull length. It is platyrostral with the depth of the maxilla approximately one third of its width at the level of the fifth maxillary alveoli. The rostrum is quite simple and lacks a median dorsal boss,

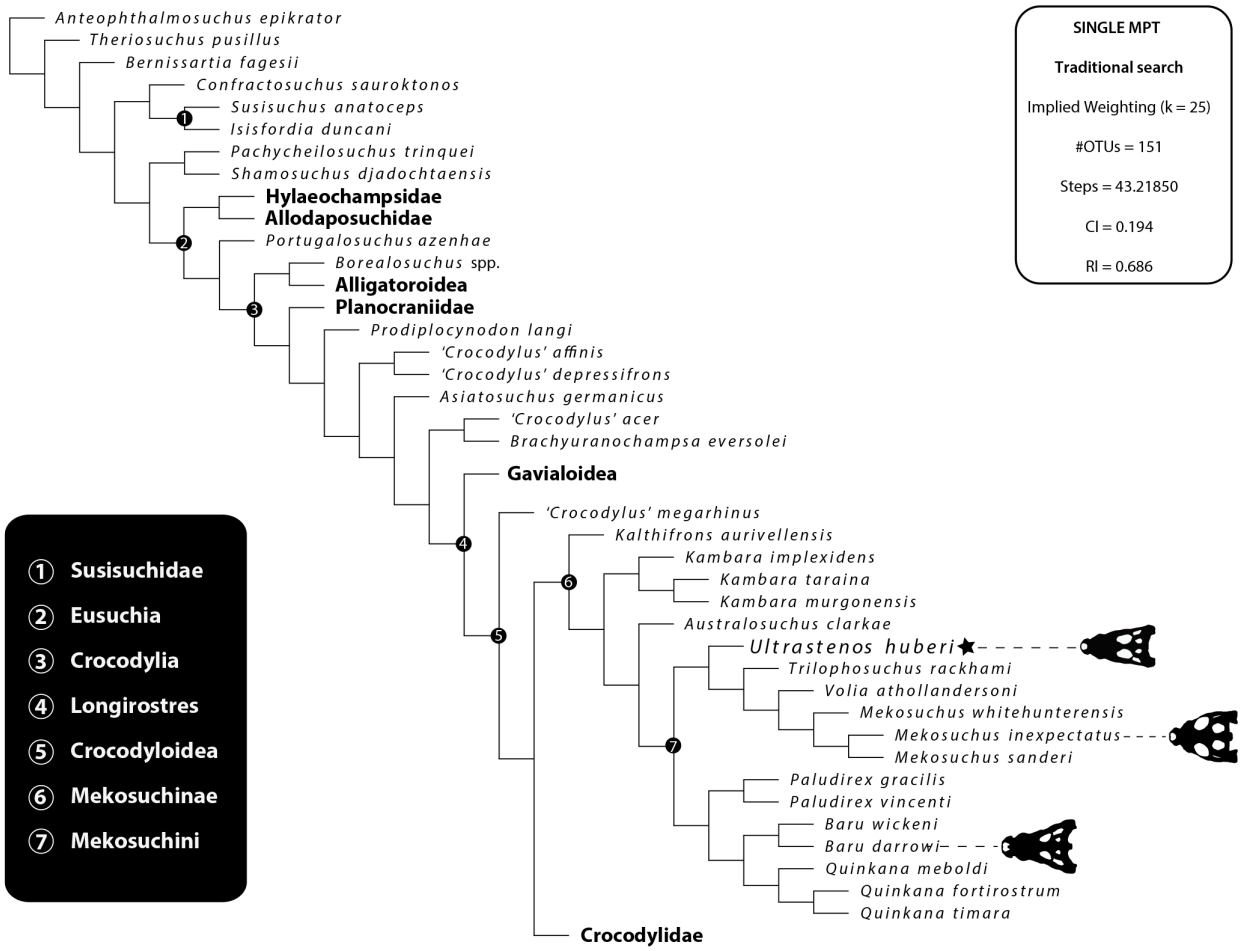

FIGURE 13. Single most parsimonious tree found by Ristevski et al. (2023) in a traditional search of their dataset using implied weights (k = 25), showing *U. huberi* sharing a more recent common ancestry with mekosuchine genera such as *Mekosuchus* than with *Baru*. Large, polyspecific, named clades that do not include Mekosuchinae have been collapsed into single branches (names in bold type) to simplify the diagram. Abbreviations: CI, consistency index; MPT, most parsimonious tree; #OTUs, number of operational taxonomic units; RI, retention index. Redrawn from figure 24 in Ristevsi et al. (2023).

anterolateral rostral ridges, and raised preorbital crests.

Dermatocranium of the dorsal skull roof. The premaxilla has a steep anterior profile due to the placement of the anterior margin of the naris close to the anterior margin of the rostrum (Figure 1C). The steepness of the profile matches that of *Baru*, however, it differs from members of that genus in being proportionally shallower (Figure 15E). The naris is slightly longer than wide, and it tilts to face anterodorsally (Figure 15E). The posterior margin of the naris lies anterior to the anterior-most extent of the maxilla. The anterior end of the bulb-shaped premaxillary fenestra is located posterior to the first pair of premaxillary alveoli while its simple, rounded posterior margin is broadly separated from the premaxilla-maxilla suture by the premaxillary symphysis (Figure 15C). The minimum interorbital distance is narrow and just under 20% of the width of the posterior cranial table (Figure 5I). The posterior cranial table bears a dorsally exposed supratemporal fossa surrounding the supratemporal fenestra with no overgrowth from the surrounding dermal bones (Figure 3A, B). The dorsal margin of this fossa is distinctive with the lateral, posterior, and medial margins forming a rounded, subcircular shape (Figures 3A, B; 5A, B). The anterior margin, however, forms an acute point that incised into the postorbital (Figure 3A, B). On the palate, the position of the anterior margin of the suborbital fenestra varies from level with the eighth maxillary alveolus (e.g., QM F31060, Figure 1B) to level with the seventh alveolus (e.g., QM F31064, Figure 15A). In both cases the anterior margin of

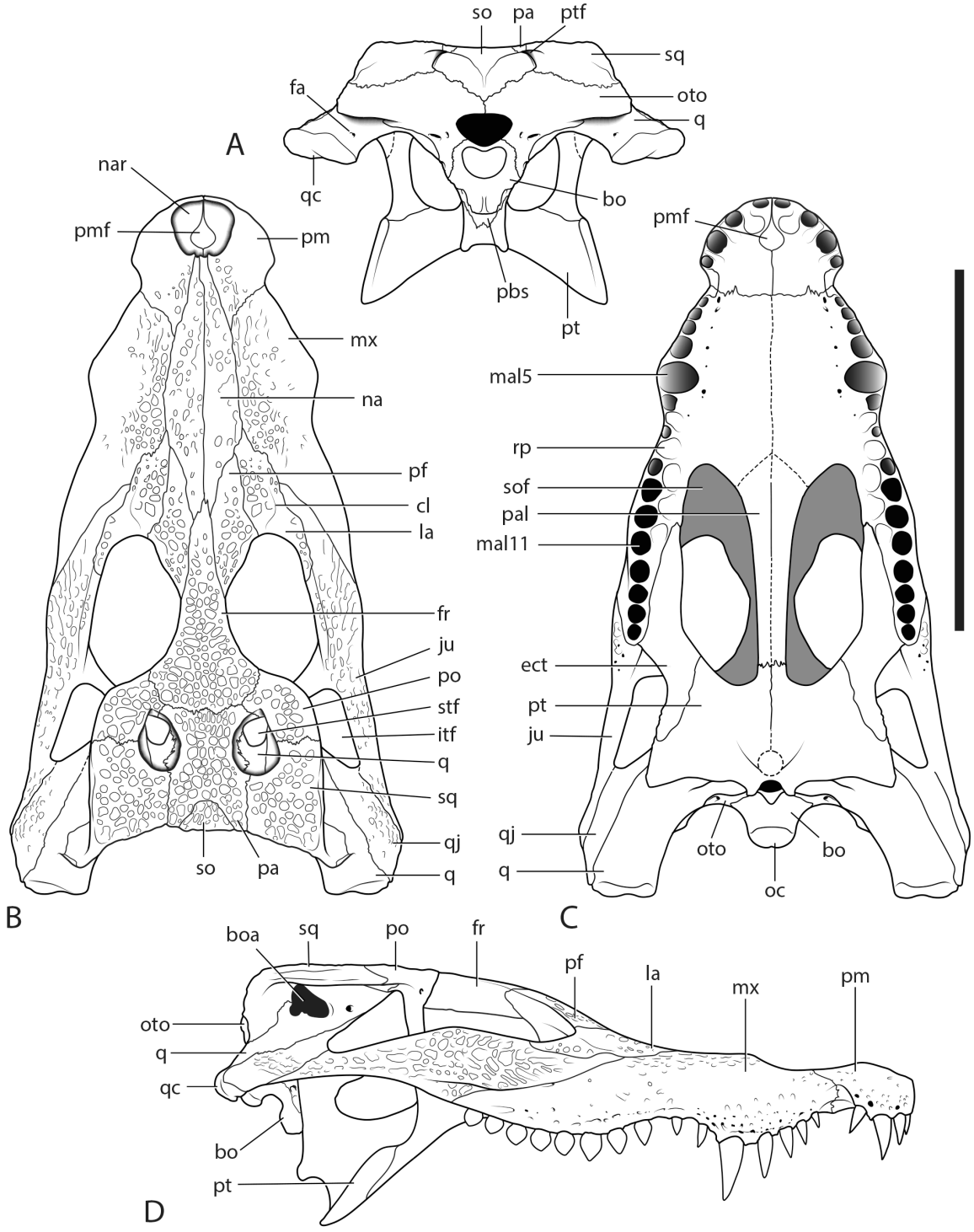

FIGURE 14. Reconstruction of *Ultrastenos huberi* based largely upon QM F31060 and QM F31076 and scaled to the size of these two specimens. A, occipital view. B, dorsal view. C, ventral view. D, right lateral view. Abbreviations: bo, basioccipital; boa, bony otic aperture; cl, canthus lacrimalis; ect, ectopterygoid; fa, foramen aëreum; fr, frontal; itf, infratemporal fenestra; ju, jugal; la, lacrimal; mx, maxilla; mal, maxillary alveolus; na, nasal; nar, naris; oc c, occipital condyle; oto, otoccipital; pa, parietal; pal, palatine; pbs, parabasisphenoid; pm, premaxilla; pmf, premaxillary fenestra; po, postorbital; pf, prefrontal; pt, pterygoid; ptf, posttemporal fenestra; q, quadrate; q co, quadrate condyle; qj, quadratojugal; rp, reception pit; so, supraoccipital; sof, suborbital fenestra; sq, squamosal; stf, supratemporal fenestra. Scale bar equals 100 mm.

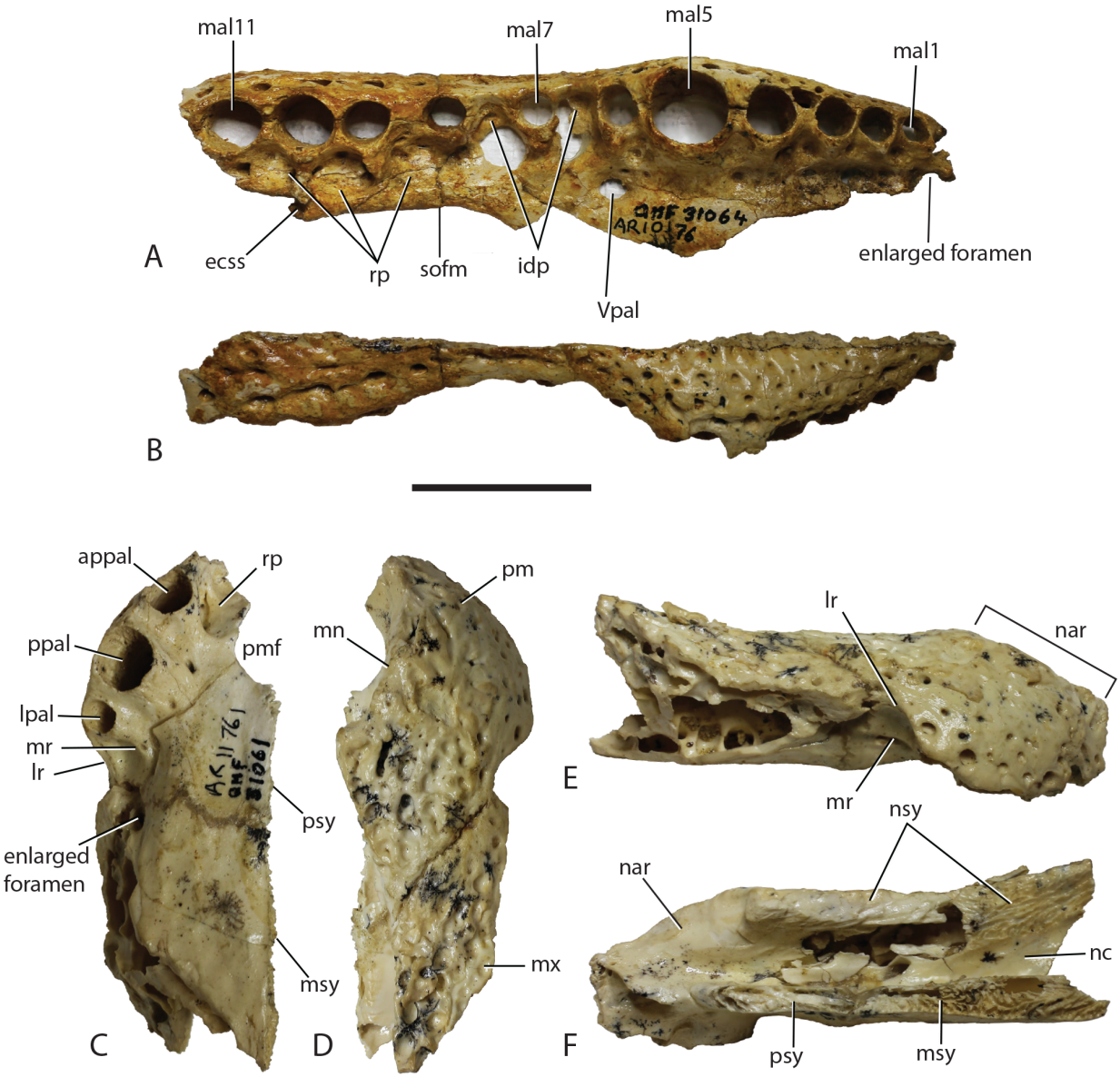

FIGURE 15. *Ultrastenos huberi*, rostral fragments. A-B, QM F31064, fragment of right maxilla. A, ventral view. B, lateral view. C-F, QM F31061, rostral fragment, including right premaxilla and fragment of right maxilla. C, ventral view. D, dorsal view. E, lateral view. F, medial view. Abbreviations: appa, antepenultimate premaxillary alveolus; ect sut, sutural surface for articulation with the ectopterygoid; idp, interdental reception pit; lpal, last premaxillary alveolus; lr, lateral ridge; mal, maxillary alveolus; mn, margin of the naris; mr, medial ridge; msy, articular surface for maxillary symphysis; nar, naris; nc, nasal cavity; nsy, articular surface for nasal symphysis; pm, premaxilla; pmf, premaxillary fenestra; ppal, penultimate premaxillary alveolus; psy, articular surface for premaxillary symphysis; rp, reception pit; sofm, margin of the suborbital fenestra; Vpal, maxillary foramen for palatine ramus of cranial nerve V_2 (maxillary division of the trigeminal nerve), note that the margins of this foramen are broken, thus enlarging the apparent size of the foramen. Scale bar equals 20 mm.

the suborbital fenestra lies anterior to the anterior orbital margins.

Known specimens have only four premaxillary alveoli but the number present at hatching is unknown. The penultimate premaxillary alveolus is the largest premaxillary alveolus, but it is smaller than the fifth maxillary alveolus (Figure 15C). The premaxillary arcade curves anteromedially so that the last alveolus is lateral to the penultimate, and the penultimate alveolus is lateral to the antepenultimate. The triangular posterodorsal processes of the premaxilla extend posteriorly to the level of the

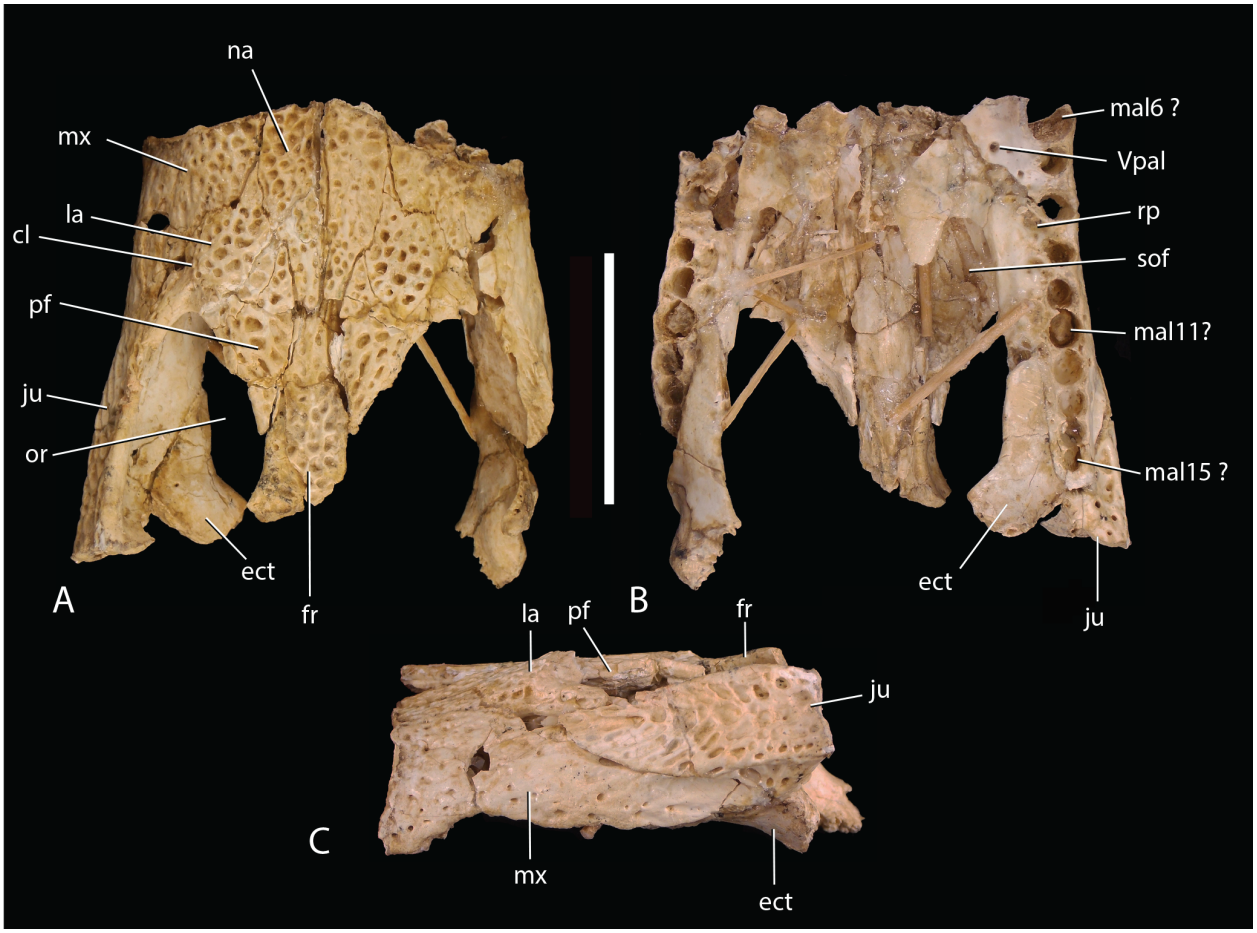

FIGURE 16. *Ultrastenos huberi*, QM F61097, cranial fragment. A, dorsal view. B, ventral view. C, left lateral view. Abbreviations: cl, canthus lacrimalis; ect, ectopterygoid; fr, frontal; ju, jugal; la, lacrimal; mal, maxillary alveolus; mx, maxilla; na, nasal; or, orbit; pf, prefrontal; rp, reception pit; sof, suborbital fenestra; Vpal, foramen for palatine ramus of cranial nerve V_2 (maxillary division of the trigeminal nerve). Scale bar equals 50 mm.

third maxillary alveoli (Figure 1A). The palatal premaxillomaxillary suture is largely transverse and lies anterior to the first pair of maxillary alveoli (Figure 15C). A ventrolaterally open arch at the lateral end of the premaxillomaxillary suture forms a notch for the reception of the fourth dentary tooth. The notch is bordered laterally and medially by a pair of ridges (Figure 15C, E).

The total number of maxillary alveoli would appear to be 15, but this interpretation hinges on the identity of the maxillary alveoli in QM F61097 (Figure 16B). We interpret the preserved alveoli of this specimen as representing the sixth through to the fifteenth, and final, alveolus. However, an alternative interpretation where the preserved alveoli represent the fifth to the fourteenth alveoli cannot be ruled out (Figure 16B). Thus, it is possible that the total number of maxillary alveoli for this species is actually 14. The first six maxillary alveoli are closely spaced and lack interdental reception pits (Figure 15A). The alveoli are bordered medially by an alveolar process (sensu Molnar, 1982). The fifth maxillary alveolus is the largest alveolus in the upper jaw and corresponds to a moderately-sized, anterior festoon (Figure 15B). A second, smaller peak of enlarged teeth occurs at the tenth and eleventh alveoli. The alveoli are unevenly spaced with noticeably larger diastemata between the sixth and ninth alveoli in comparison to the rest of the tooth row but are evenly and closely spaced posterior to the tenth alveolus (Figures 15A, 16B). All, but the last, of the maxillary alveoli are subcircular, indicating a lack of labio-lingual compression of the maxillary teeth. The alveolar row continues to the level of the posterior margin of the suborbital fenestra, without a substantial non-dentigerous process of the maxilla posterior to the last alveolus. A pair of deep interdental reception pits occupy the spaces anterior and posterior to the seventh maxillary alveolus, whereas a series of three shallower

medial pits occurs posterior to these between the level of the eighth and eleventh alveoli. The part of the maxillary palate that bears these reception pits is narrow, with the distance from the suborbital fenestra to the medial side of the maxillary alveoli subequal to the width of the tenth alveolus, when measured at the level of the tenth alveolus (Figure 15A). There are no reception pits posterior to the eleventh aveolus (Figure 16B). The foramen for the palatine ramus of the trigeminal nerve (located ventromedial to the fifth alveolus) is less than 20% of the diameter of the sixth maxillary alveolus (Figure 1B). The maxillary margin of the suborbital fenestra is straight and does not bow medially into the fenestra. Dorsally, the maxilla lacks a posterior spur either inserting into the lacrimal or between the lacrimal and the nasal and there is a long nasolacrimal suture (Figure 16A).

The nasals extend all the way to the posterior margin of the naris but do not protrude into it (Figure 1A). The lacrimal is wider than the prefrontal with a maximum transverse width that is 1.28 times that of the latter (Figure 16A). An unornamented, shallow sulcus on the dorsal surface of the lacrimal extends from the anterior apex of the orbit to the anterolateral margin of the lacrimal (Figure 16A). This sulcus divides the lacrimal ornamentation into a posterolateral region adjacent to the lateral margin of the orbit and an anteromedial region adjacent to the prefrontal and nasal. The medial margin of the sulcus forms a weak ridge that divides the higher anteromedial region from the descending posterolateral region, thus forming a subtle ridge similar to the more pronounced version present in *B. wickeni* (Yates, 2017: figure 7, labelled 'preorbital ridge'). Rio and Mannion (2021: appendix 2) distinguished two distinct forms of preorbital ridge which they treated as two independent characters (characters 27 and 30) in their matrix. The first of these (character 27) is the type seen in *U. huberi* and *B. wickeni,* where there is an angulation caused by the junction of two planar surfaces, without a projecting ridge. They somewhat confusingly applied the name 'canthus rostralis' to this type of ridge. 'Canthus rostralis' had been used previously (Brochu, 1999) for non-homologous oblique ridges that occur on the dorsal rostral surface of some caimanines. They then restricted the term 'preorbital ridge' to those structures for which there is a dorsal projection of bone on the lacrimal, built above the dorsal surface of the preorbital rostrum (character 30). This type of preorbital ridge most notably occurs in some species of *Crocodylus* (e.g., *C. porosus*). To avoid confusion we apply a new, more precise, nomenclature to these different ornamental features. We continue to use 'canthus rostralis' in the sense that Brochu used it, i.e., for the oblique rostral ridges seen in some caimanines (Brochu, 1999, fig. 61). For the two distinct types of 'preorbital ridge' we employ two new terms: the crista preorbitalis (preorbital crest) for the raised ridges, of the type seen in *C. porosus*, and canthus lacrimalis (lacrimal ridge) for the ridge formed from the meeting of two angled, planar surfaces such as is seen in *U. huberi* (Figures 1A, 16A).

The anterior termination of the lacrimal forms an acute, narrow process that lies anterior to the prefrontal. The anterior termination of the prefrontal lies anterior to the anterior process of the frontal, which in turn lies anterior to the level of the anterior margins of the orbits (Figure 16A). The anterior process of the frontal of the holotype forms an acute point that inserts between the posterior ends of the nasals for a distance of just under 5 mm (Figure 1A) whereas the termination is broader in QM F F61097 and fails to insert between the nasals at all (Figure 16A). The frontal-nasal contact prevents the prefrontals from contacting each other. The prefrontal orbital margin is simple, lacking raised bosses, a linear sulcus or a laterally projecting bevelled flange. The dorsal surface of the frontal is flat and flush with the orbital margins. There is no sagittal keel on the frontal or parietal (Figure 5A). The frontoparietal suture lies entirely on the skull roof and does not reach the supratemporal fossa (Figures 3B, 5A). The suture is bowed posteriorly and varies from shallowly bowed (QM F31076; Figure 5A) to deeply bowed (QM F31075; Figure 3A, B).

The anterior termination of the jugal lies slightly anterior to the anterior orbital margin and the anterior process of the frontal (Figure 16C). Ventrally the anterior ramus of the jugal, adjacent to the maxilla and immediately posterior to it, bears a ventrally-facing surface that bears several ornamental pits, similar to those found on other parts of the dorsal skull roof (Figure 16B, C). Medially, there are a pair of enlarged foramina anterior to the base of the postorbital bar. In lateral view, the ventral margin of the lower temporal bar is mildly concave (Stein et al., 2016b, fig. 1g). The postorbital forms the dorsal part of the slender postorbital bar. It has a rounded cross-section and lacks an anterior protuberance.

The lateral side of the squamosal forms a narrow vertical surface with a single central sulcus that maintains subparallel margins for its length (Figures 3A, B; 11A). The floor of this sulcus is smooth

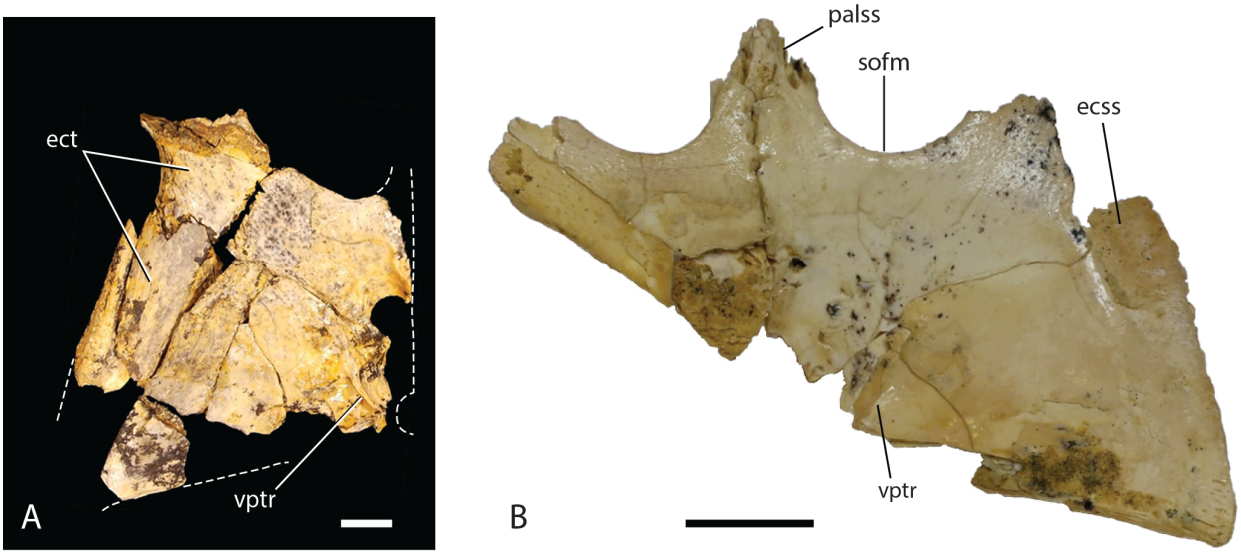

FIGURE 17. *Ultrastenos huberi*, pterygoid fragments. A: QM F42665, right pterygoid in articulation with right ectopterygoid in ventral view. B: QM F31076, pterygoid pair in ventral view. Abbreviations: ect, ectopterygoid; ecss, sutural surface for articulation with the ectopterygoid; palss, sutural surface for articulation with the palatine; sofm, margin of the suborbital fenestra; vptr, ventral pterygoid ridge. Scale bar equals 10 mm.

and unornamented. Posteriorly the short posterolateral process of the squamosal descends steeply towards the dorsolateral corner of the paroccipital process, so that its dorsal profile forms a near right-angle with the dorsal surface of the skull table. There is no lamina of the squamosal extending ventrolaterally from the lateroventral corner of the paroccipital process over the dorsal surface of the quadrate. Given the anterior attenuation of the quadratojugal sutural scar on the quadrate, the anterior end of the quadratojugal probably terminates on the posterior dorsal margin of the infratemporal fenestra and fails to reach the postorbital (Figure 3A-D). Posteriorly, the quadratojugal completely covers the lateral surface of the quadrate condyle.

Dermatocranium of the palate. The palatine is proportionally wide at the anterior end of the palatal bar, comprising over 30% of the total with of the rostrum at the level of the eighth alveolus (Willis, 1997, fig. 11), thus constricting the width of the suborbital fenestrae at this level. The anterior palatine process is relatively short, extending just slightly anterior to the suborbital fenestra, based on the extent of the maxillary symphysis QM F61097. The anterior tip of the maxillary ramus of the ectopterygoid forms a single point that intrudes slightly into the maxilla so that the maxilla separates the first 1.5 mm of the ectopterygoid from the margin of the suborbital fenestra (Figure 15A). Although the maxillary margin of the suborbital fenestra is straight, the medial margin of the maxillary ramus of the ectopterygoid is slightly bowed medially at the level of the thirteenth to fourteenth alveoli (Figure 16A, B). This ramus extends for just under two thirds of the length of the suborbital fenestra and has an approximately equilaterally triangular cross-section. The lateral margin of the ramus extends parallel and close to the maxillary tooth row but does not contribute to the medial walls of any maxillary alveoli. Posteroventrally, the tip of the pterygoid ramus of the ectopterygoid fails to reach the posterior tip of the pterygoid flange (Figure 17A, B). The pterygopalatine suture is placed well anterior of the posterior margin of the suborbital fenestra, indicating that the pterygoids contributed just over 10% of the length of the palatal bar (Figures 14C, 17B). The ventral surface of the pterygoid bears an anteriorly directed ridge extending from the lateral margin of the choana (Figure 17A, B).

Splanchnocranium. The quadrate forms the floor of the anterior temporal foramen inside the supratemporal fossa, which keeps the squamosal and the parietal widely separated (Figures 3B, 5A). The anterior end of the quadrate contacts the medial side of the postorbital bar at its dorsal end. The quadrate sends a small bony process up the weakly bowed posterior margin of the bony otic aperture (sensu Montefeltro et al., 2016; Figure

4B). A broad, occipitally-facing surface of the medial process of the quadrate is exposed ventrolateral to the otoccipital (Figure 3D). There is a roughly triangular ventral excursion of the quadrate-pterygoid suture on the lateral braincase wall (Figure 4D). A small, but distinctly visible, quadrate foramen aëreum opens on the flattened medial side of the dorsal surface of the posterior ramus of the quadrate (Figure 3C, D). This ramus is short, with the distance between the paroccipital process and the quadrate condyle less than the transverse width of the condyle (Figure 12 A, E). The dorsomedial margin of the quadrate condyle, when viewed normal to its articular surface, is flattened, with a straight section extending for approximately a quarter of the mediolateral width of the condyle (Figure 18A). No concave notch like the one seen in *M. inexpectatus* (Rio and Mannion, 2021: Appendix 2, figure 45c) is present, but the shape seen here would appear to be intermediate between the notched condition and the convex dorsomedial corner seen in *B. wickeni* (Figure 18B). The dorsal margin of the condyle is concave, producing a medial constriction between the lateral and medial hemicondyles (Figure 18A).

Chondrocranium. The supraoccipital forms a large, trapezoidal dorsal exposure that greatly restricts, but does not eliminate, the parietal contribution to the occipital margin of the skull table (Figure 3A, B). The straight, to gently convex, posterior margin of the supraoccipital hides the postoccipital processes in dorsal view. The otoccipital forms a vertical occipital face that is hidden in dorsal view. The posterior medial process of the otoccipital is reduced. In QM F31075 it is so reduced that it terminates anterior to the occipital condyle (Figures 3C, D; 12H) whereas in QM F42665 the otoccipital-basioccipital suture grazes the dorsolateral corner of the occipital condyle (Figure 12D). The posterior carotid foramen opens on the occipital surface of the otoccipital, far ventral to the opening of the metotic foramen and the posterior hypoglossal foramen (Figure 3D). The acute ventral termination of the otoccipital reaches the dorsal margin of the basal tuber (Figure 3D). The occipital plate of the basioccipital is dorsoventrally deeper than the occipital condyle and has lateral margins that converge ventrally. This plate bears an exceptionally tall sagittal keel at its ventral end (Figure 12C, G). The ventral margin of the plate is straight in occipital view. The pharygotympanic foramen opens on the lateral margin of the basioccipital plate, dorsal to the level of the median pharyngeal tube foramen (Figure 3D). The parabasisphenoid forms a dorso-

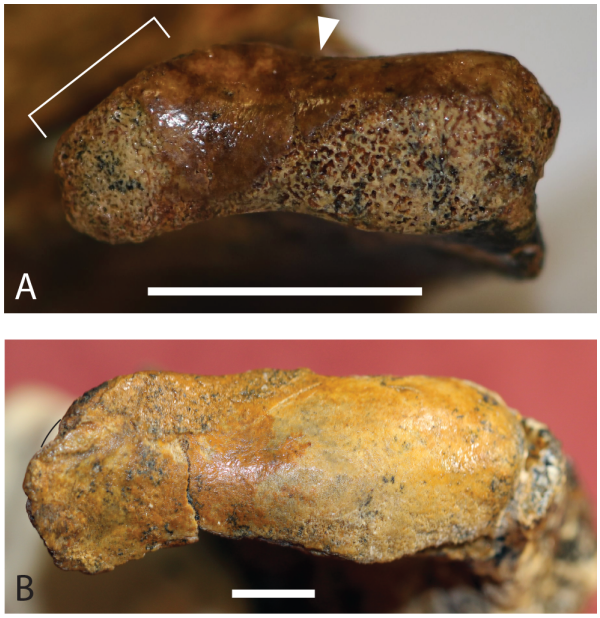

FIGURE 18. Quadrate condyles of *Ultrastenos huberi* and *Baru wickeni* compared. A: *Ultrastenos huberi*, QM F31075, right quadrate condyle, photograph taken normal to the articular plane of the quadrate condyle (dorsal is towards the top of the page). The flattened dorsomedial margin is marked by a rectangular bracket and the dorsal indentation between the medial and lateral hemicondyles is marked by triangular arrow. B: *Baru wickeni*, NTM P911, right quadrate condyle, photograph taken normal to the articular plane of the quadrate condyle (dorsal is towards the top of the page). Note that the flattened dorsomedial margin, and the dorsal indentation are absent. The small notch visible on the medial margin is due to damage. Scale bar equals 10 mm.

ventrally deep exposure anterior to median pharyngeal tube foramen and ventral to the basioccipital (Figure 3D). This exposure of the parabasisphenoid is flanked by dorsoventrally tall posterior processes of the pterygoid. The parabasisphenoid is also exposed on the lateral surface of the braincase where its anterior suture with the pterygoid is recessed within a sulcus that parallels the posterolateral margin of the braincase (Figures 4C, D; 12C, G). Anteriorly the parabasisphenoid is exposed ventral to the laterosphenoids where it bears the anteriorly projecting parabasisphenoid rostrum. The base of the rostrum is simple and is not flanked on each side with a sulcus (Figure 4D). This anterior exposure of the parabasisphenoid does not extend onto the lateral braincase wall, anteroventral to the trigeminal foramen (Figure 4D). The anterior margin of the capitate process of the laterosphenoid is oblique and oriented anteromedially (Figures 4D, 5B). The laterosphenoid

forms two complete bridges over the cavum epiptericum, the robust lateral bridge sutures to the pterygoid while the caudal bridge sutures to the quadrate. There is moderate exposure of the prootic around the trigeminal foramen within the cavum epiptericum (Figure 4D).

Mandible. The first and second pairs of dentary teeth are steeply angled anterodorsally (Figure 19B). The third dentary tooth is smaller than the fourth, which forms a large canine peak (Figures 19A-C; 20A, D). The third and fourth alveoli are closely spaced and almost in contact but are not confluent (Figure 20A), while the fifth to seventh alveoli, posterior to the fourth alveolus, are closely packed and lack diastemata (Figure 20A, D). The posterior festoon reaches a level higher level to the anterior (Figure 20B), although this is barely the case in QM F31068 (Figure 20E). The peak of the posterior festoon coincides with the tenth to eleventh alveoli, with the eleventh being the larger of the two (Figures 19A, B; 20A, B). Further posterior, the dentary narrows into a straight alveolar row. The total number of dentary alveoli is unknown but reconstruction from non-joining fragments indicates that there were at least 16 alveoli (Figure 19A-C). The dentary symphysis extends posteriorly so that it is level with the sixth alveolus (e.g., QM F31069) or the margin between the fifth and sixth alveoli (QM F31068; Figures 19A; 20A, D). The lateral surface of the dentary curves smoothly onto the ventral surface with no prominent ventrolateral ridge. The posterior end of the symphyseal surface is bilobed in medial view with the dorsal lobe extending posterior to the ventral lobe (Figures 19B, 20E). The anterior end of the splenial fails to make contact with the mandibular symphysis and terminates at the level of the seventh and eighth alveoli (Figure 20C, E, F). The anterior termination is bifurcated with processes lying alternately dorsal and ventral to the Meckelian sulcus (Figures 19B, 20C). In QM F3169 the dorsal process is abbreviated so that the tip of the ventral process lies anterior to the dorsal process (Figure 20F), whereas the sutural scars for each process are level with one another in QM F31068 and QM F61096 (Figure 20C, E). Although the posterior end of the splenial is not preserved the shape of the dentary and the surangular indicate that the posterior dorsal profile of the splenial would have been straight.

Posteriorly, the mandible bears a small, oval, external mandibular fenestra with a ventral margin that weakly indents the dorsal margin of the angular (Figures 2H, 19C). Its length is approximately 20% of the distance between the mandibular glenoid and the posterior end of the dentary tooth row. A posterodosal process of the dentary extends along the dorsal margin of the external mandibular fenestra and terminates posterior to its posterodorsal corner (Figures 2E, 19C). The dorsal margin of the right angular of QM F42665 indicates that the surangular-angular suture intersects with the margin of the external mandibular fenestra on its posterior margin (Figure 2H). The margins of the ornamented area on the posterior mandible do not form laterally everted ridges. The smooth fossa for the origin of the *M. pterygoideus ventralis* on the angular is visible laterally, posteroventral to the ornamented part of this bone. The surangular bears a tall ascending process on the lateral side of the posterior wall of the glenoid fossa (Figure 2E). There are no fossae on the dorsal surface of the surangular, adjacent to the glenoid fossa. No anterior spur of the surangular can be seen bordering the lingual side of the posterior most dentary alveoli, but it may be masked by poor preservation. The angulosurangular suture on the internal wall of the adductor chamber contacts the articular at its anterior tip. The lingual foramen for the articular and alveolar nerve on the internal wall of the adductor chamber opens on the articulosurangular suture. Within the glenoid fossa, the surangular makes a straight suture with the articular (Figure 2I). The posterior process of the surangular of QM F42665 is broken anterior to its termination but remains broad along its length and shows no sign of having pinched off anterior to the posterior end of the retroarticular process. The moderately elongate retroarticular process is posterodorsally directed but the posterior dorsal tip does not extend dorsal to the level of the posterior margin of the glenoid fossa (Figure 2E).

Remarks

Willis (1997) listed several paratypes of *'B.' huberi.* These do not help unite 'cranial form 1' with *U. huberi* or bolster the case for the synonymy of *U. willisi* and *U. huberi*, but they do improve our knowledge of the osteology of the species and have been used in the description above. However, not all of the paratypes can be justifiably referred to *U. huberi*. The significantly informative paratypes are discussed here with justifications for their inclusion or exclusion form the hypodigm of *U. huberi*.

QM F31061 is a rostral fragment that includes the right premaxilla and part of the right maxilla (Figure 15C-F). It can be referred to *U. huberi* on the basis of the ridges developed along the medial

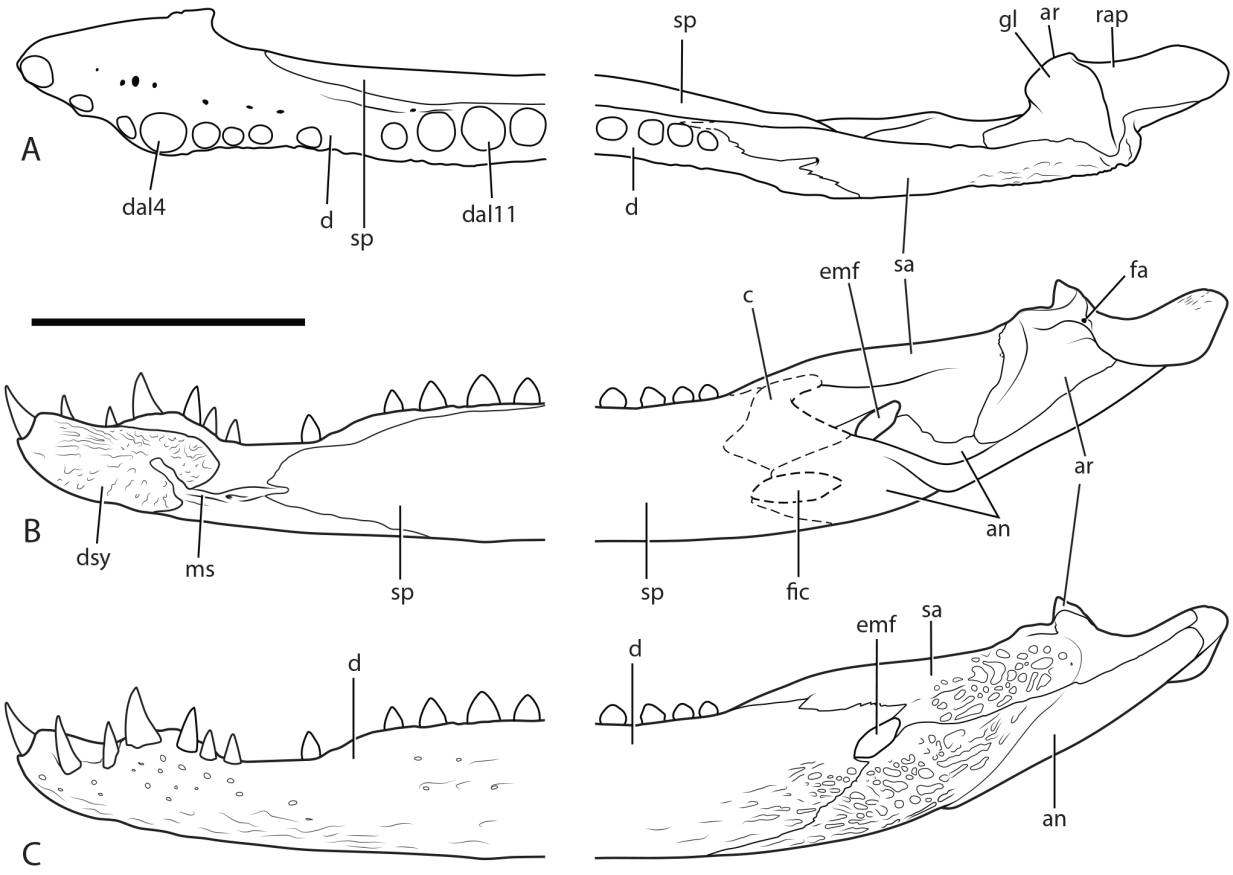

FIGURE 19. *Ultrastenos huberi*, reconstructed left mandibular ramus based largely upon QM F61096 and QM F42665, scaled to the size of the former. A, dorsal view. B, medial view (reversed for comparison). C, lateral view. Abbreviations: an, angular; ar, articular; c, coronoid; d, dentary; dal, dentary alveolus; dsy, symphyseal surface of the dentary; emf, external mandibular fenestra; fa, foramen aëreum; fic, foramen intermandibularis caudalis; gl, mandibular glenoid; ms, Meckelian sulcus; rap, retroarticular process; sa, suraqngular; sp, splenial. Scale bar equals 50 mm.

and lateral margins of the lateral premaxilla-maxilla notch, the enlarged anterior maxillary neurovascular foramen and an anteriorly placed, transverse premaxilla-maxilla suture that can be projected to have been anterior to the first maxillary alveolus. It is important to note that the lateral ridge, which we propose to be an autapomorphy for the species, has been erased from the left side of the holotype due to erosion of the bone surface. It nonetheless remains present and visible on the right side.

QM F31062 (Figure 21A-C) is an incomplete, juvenile premaxilla that is significant for retaining a small second alveolus close to the medial margin of the third for a total of five alveoli (Figure 21A). However, the margins of the lateral premaxilla-maxilla notch are rounded, the anterior profile of the premaxilla is relatively deeper and the external naris lacks a strong anteroventral tilt in lateral view (Figure 21C). For these reasons the specimen is identified as a juvenile *Baru wickeni* and removed from the hypodigm of *U. huberi*.

The paratypes include two incomplete maxillary specimens, QM F31063 (Figure 21D, E) and F31064 (Figure 15A, B) that differ in some taxonomically significant ways. Firstly, both preserve the sutural articulation facet that receive the anterior end of the ectopterygoid. In QM F31063 this articulation intrudes deeply into the maxilla so that the anterior tip of the ectopterygoid (when in articulation) is separated from the margin of the suborbital fenestra by a lamina of the maxilla, which has a length of just over one adjacent alveolus (Figure 21D). A deeply intruding anterior ectopterygoid tip is an autapomorphic feature of *Baru wickeni* (Yates, 2017). The ectopterygoid articulation of QM F31064 is also inset but in contrast to QM F31063, the inset is minimal with the anterior tip of the ectopterygoid separated from the margin of the suborbital fenestra by a tiny triangular process of

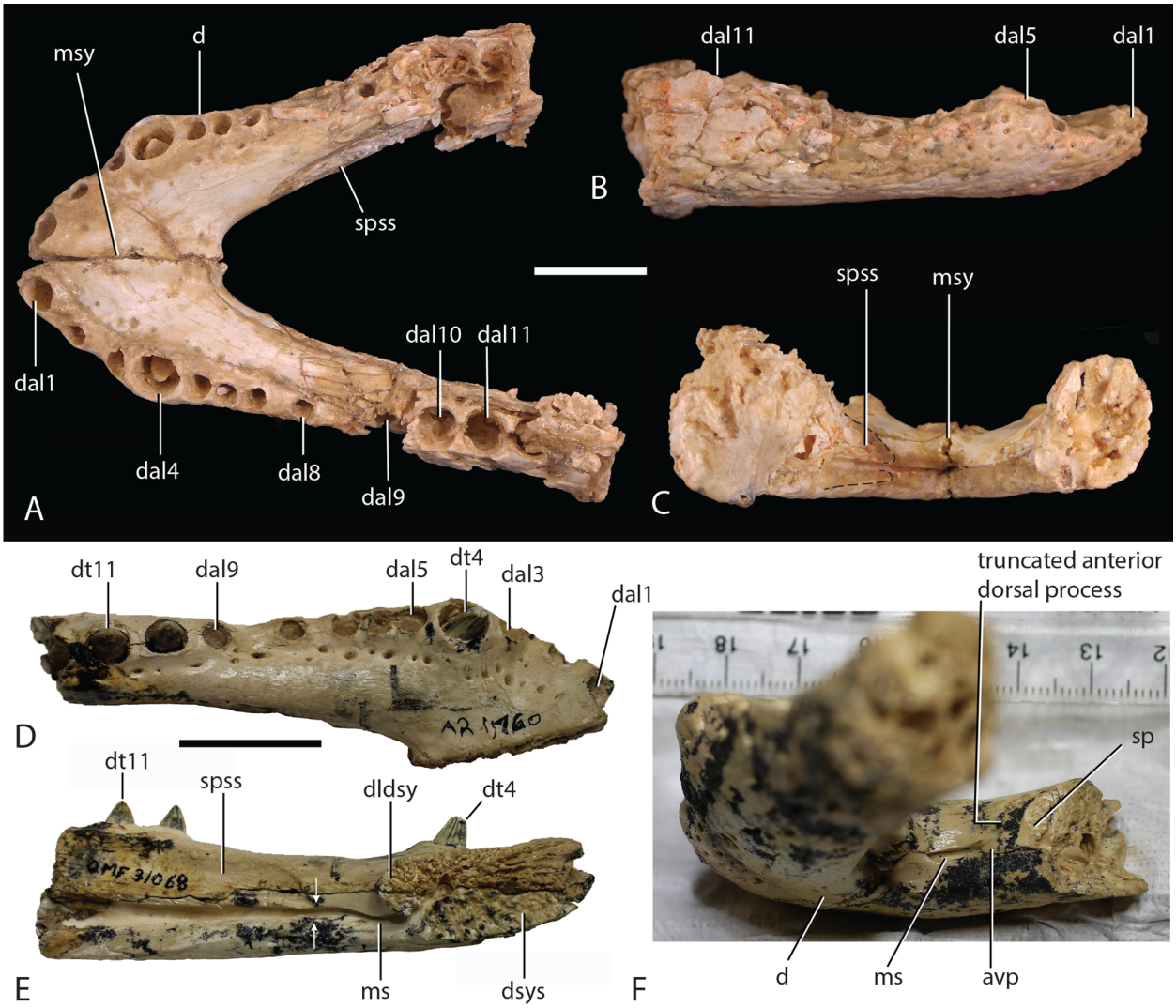

FIGURE 20. *Ultrastenos huberi*, anterior mandibular fragments. A-C: QM F61096, articulated left and right dentaries. A, dorsal view. B, right lateral view. C, posterior view. Dashed line in (C) represents the anterior margin of the splenial sutural scar. D, E: QM F31068, left dentary fragment. D, dorsal view. E, medial view. White arrows in (E) indicate the anterior tip of the dorsal and ventral anterior splenial processes. F: QM F31069, symphyseal fragment of mandible in posteriomedial view. Abbreviations: avp, anterior ventral process of the splenial; d, dentary; da, dentary alveolus; dldsy, dorsal lobe of the dentary symphyseal surface; dsys, symphyseal surface of the dentary; dt, dentary tooth; ms, Meckelian sulcus; msy, mandibular symphysis; sp, splenial; spss, sutural surface for articulation with the splenial. Scale bar equals 20 mm.

the maxilla, with a length of just over 10% of the length of the adjacent alveolus (Figure 15A). The alveoli of QM F31063 exhibit marked labio-lingual compression, especially from the ninth alveolus backwards (Figure 21D), a feature seen in juvenile specimens of *B. iylwenpeny* (Yates et al., 2023). In contrast the alveoli of QM F31064 are subcircular as far back as the eleventh alveolus (Figure 15A). QM F31063 also shows a moderately large foramen ventromedial to the fifth alveolus for the palatine ramus of the trigeminal nerve, a characteristic seen in *Baru* (Yates et al., 2023) but not the holotype of *U. huberi*. The size of the foramen in QM F31064 cannot be determined due to breakage around the margins of the foramen. Finally, the ventral margin of the sutural surface for articulation with the jugal of QM F31063 is produced into a sharp lateral keel, suggesting that it supported a lateral flange on the jugal, which is another autapomorphy of *B. wickeni* (Yates, 2017). Unfortunately, the homologous region of QM F31064 is missing. From these observations, QM F31063 is removed

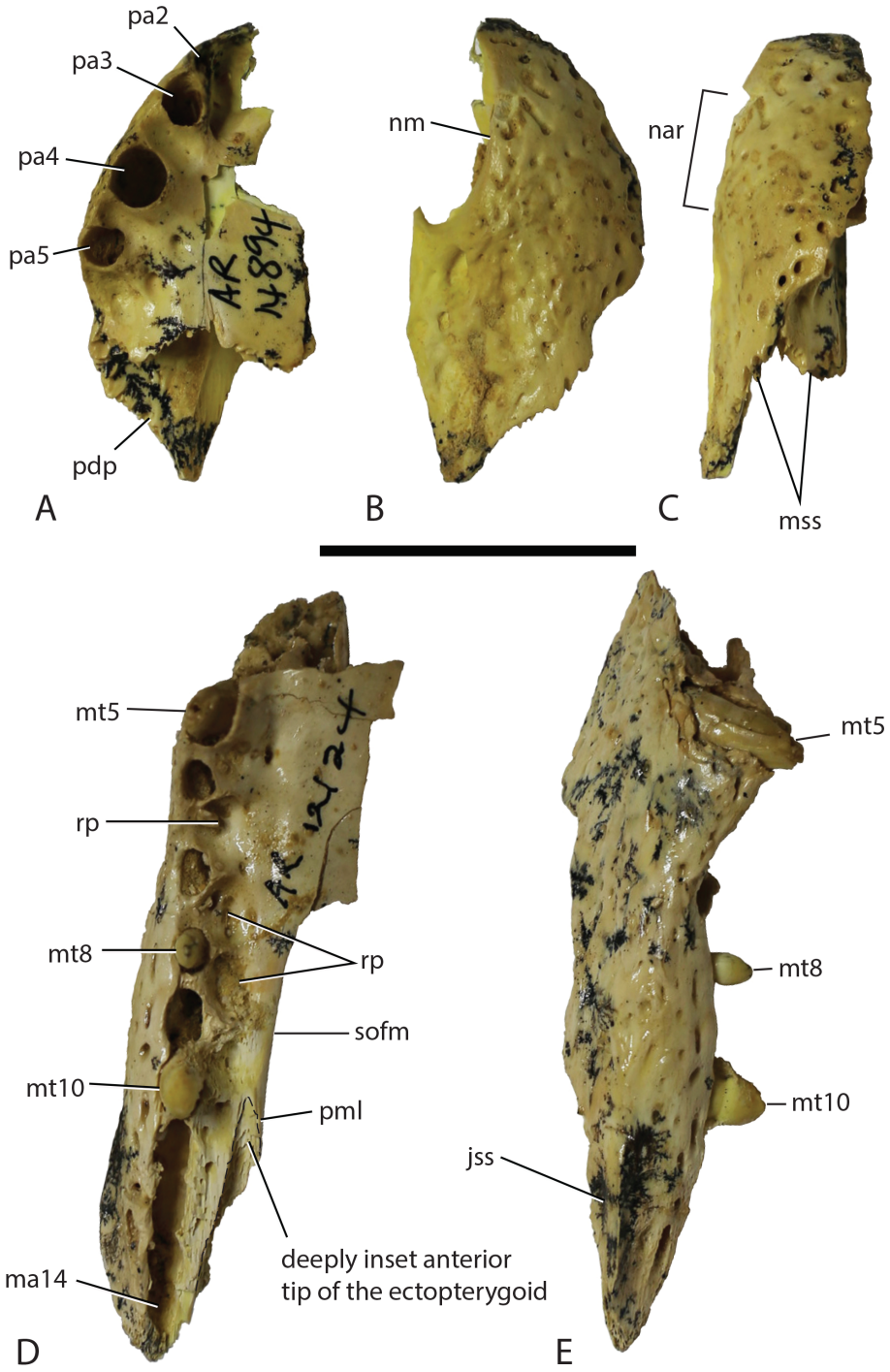

FIGURE 21. *Baru wickeni*, bones from the maxillary rostrum of small juveniles. A-C: QM F31062, right premaxilla. A, ventral view. B, dorsal view. C, lateral view. D, E: QM F31063, posterior fragment of right maxilla. D, ventral view. E, lateral view. The dashed line in (D) represents margins of the ectopterygoid sutural scar. Abbreviations: jss, sutural surface for articulation with the jugal; ma, maxillary alveolus; mss, sutural surface for articulation with the maxilla; mt, maxillary tooth; nar, naris; nm, narial margin; pa, premaxillary alveolus; pdp, posterior dorsal process of the premaxilla; pml, posterior medial lamina of the maxilla; rp, reception pit; sofm, margin of the suborbital fenestra. Scale bar equals 20 mm.

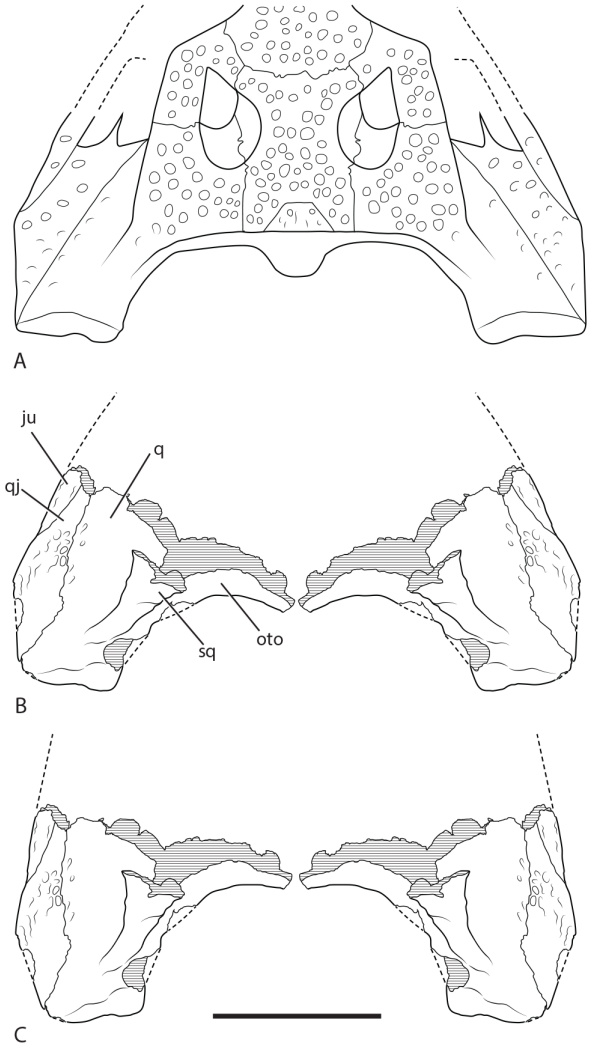

FIGURE 22. Reconstruction of the posterior skull of *Ultrastenos huberi*. A: Composite reconstruction showing marked anterior narrowing congruent with the slender longirostrine morphotype. Redrawn from Stein et al. (2016). B, C: QM F42665, temporal fragment from the holotype of *U. willisi*, mirror imaged to create reconstructions. B, temporal fragment arranged to match the reconstruction in (A). C, Alternative arrangement of the temporal fragment to match the brevirostrine reconstruction of *U. huberi* supported here. Abbreviations: ju, jugal; oto, otoccipital; q, quadrate; qj, quadratojugal; sq, squamosal. Hatched areas represent broken bone surfaces. Scale bar equals 50 mm.

from the hypodigm of *U. huberi* and is identified as a juvenile specimen of *B. wickeni*. QM F31064 is retained in *U. huberi* on the basis of its enlarged anterior maxillary neurovascular foramen.

Willis (1997) also assigned three anterior mandibular specimens (QM F31067, F31068 and F31069) to *'B.' huberi.* The basis for these referrals was that the mandibles of the other three crocodylian species present in the White Hunter Local Fauna were known and were demonstrably distinct from those that were referred to *U. huberi* (Willis, 1997), which is a line of reasoning that is accepted here. Willis (1997) also noted that QM F31068 (Figure 20D, E) is an almost exact fit for the holotype of *U. huberi*, further supporting this referral.

Finally, we refer two previously unmentioned specimens to *U. huberi*. The first of these, QM F61096 (Figure 20A-C), is a conjoined pair of dentaries that are referred to *U. huberi* for the same reason that QM F31067, F31068 and F31069 are referred to this species. Secondly, there is QM F61097 (Figure 16A-C), which includes the orbital region of the skull and provides anatomical details not seen in any other specimen referred to *U. huberi*. It can be referred to *U. huberi* on the basis of the distinctive dorsal ornamentation that is shared with QM F31060, F31075, and F31076 and that it can be clearly excluded from *Baru wickeni*, *Mekosuchus whitehunterensis* and *Quinkana meboldi*. The taxonomic referrals made in this paper are summarised in Table 2.

DISCUSSION

We have argued here that the holotype rostrum of *Baru huberi* belongs to the same individual as QM F31076, which had been previously labelled as 'WH cranial form 1'. If this association turns out not to be correct we have still provided compelling evidence that the two belong to the same species. In the unlikely event that even this is found to be incorrect, then the existence of the new *Ultrastenos* species from Bullock Creek would nonetheless strongly imply that *'Baru' huberi* and 'WH cranial form 1' would have to originate from closely related and morphologically similar species. Furthermore, the mandible of the Bullock Creek taxon (Figure 10D) is, by itself, sufficient to demonstrate that *Ultrastenos* is a brevirostrine taxon, supporting the reassignment of morphological type proposed here, independent of the taxonomic changes. If the reconstruction of *U. huberi* presented here (Figure 14A-D) is accepted, then how can the features indicative of slender longirostry, as outlined by Stein et al. (2016b), be explained? The slender longirostrine reconstruction (Stein et al., 2016b) rests largely on an apparent constriction of the dentigerous portion of the mandible in comparison to the postdentary portion. The relevant parts of the holotype are not conjoined, and the apparent constriction rests upon reconstruction of the cranium and mandible (Figure 22A, B). An alternative recon-

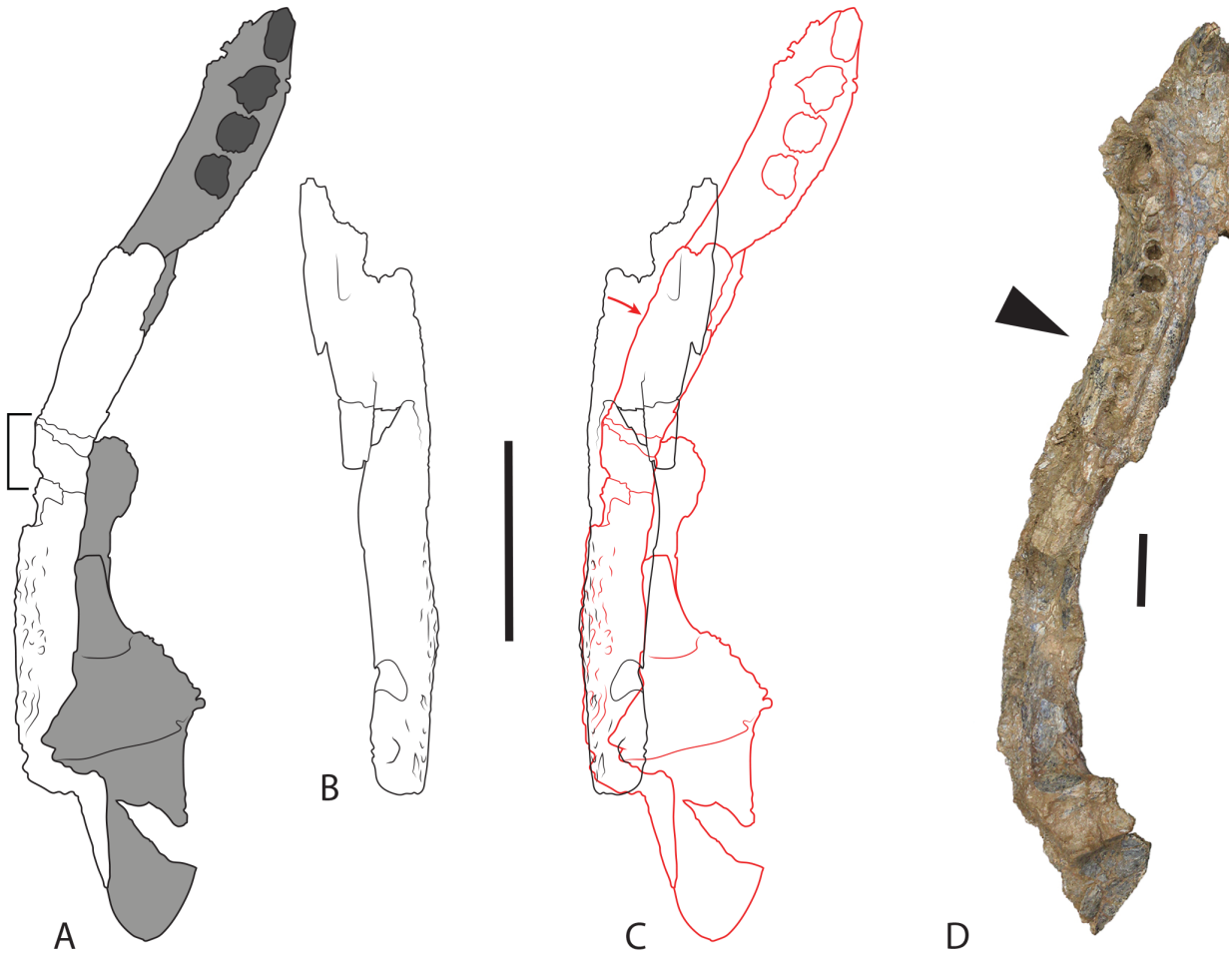

FIGURE 23. Curvature of the mandible of *Ultrastenos huberi* compared to *Baru iylwenpeny* Yates et al. A-C: *Ultrastenos huberi*, QM F42665, mandibular fragments. A, posterior fragment of the left mandibular ramus. B, right surangular. C, mirror image of the right surangular overlain onto the left mandibular ramus fragment (drawn in red). The left surangular in (A) is filled with white, the other bones are shaded grey. The rectangular bracket in (A) indicates a highly fractured and re-glued zone. Note the offset of the end anterior of the left ramus in (C), which has rotated medially relative to the right surangular (marked with red arrow). D: *Baru iylwenpeny*, NTM P2787, right mandibular ramus (image reversed). The triangle indicates an inflection point similar to that exhibited in QM F42665. Scale bar equals 50 mm.

struction rotates the quadrate/quadratojugal fragment anterolaterally so that the lateral margin of this piece converges anteriorly at a shallower angle and realigns the axis of the quadrate condyle (Figure 22C). Furthermore, the more complete left mandibular fragment has been reassembled and the anterior portion would appear to be slightly bent anteromedially relative to the posterior portion, accentuating the apparent anterior constriction of the mandible (Figure 23A). This can be seen when the right surangular fragment is reflected and overlain on the left mandibular ramus (Figure 23B, C). Stein et al. (2016b) also stated that the lateral bowing of the mandibular rami is suggestive of anterior constriction; however, such bowing is also present in some brevirostrine mekosuchines such as *B. iylwenpeny* (Figure 23D). The apparent shallow posterior mandible and straight dorsal margin of the surangular may argue against altirostry but do not distinguish slender longirostry from platyrostry. As has already been discussed, *U. huberi* is a remarkably platyrostral species especially in comparison to contemporary species of *Baru, Mekosuchus,* and *Quinkana.* While it is true that the retroarticular process of the type specimen of QM F42665 is more elongate than some other mekosuchines (e.g. *Mekosuchus whitehunterensis*: Willis, 1997, figure 5; *Baru iylwenpeny*: Yates et al., 2023, figure 33a) it is not diagnostic of slender longirostry. The proportion of its length to the width of the glenoid (1.17) overlaps with several non-longirostrine crocodylians such as *Alligator mississippiensis*

TABLE 2. Late Oligocene crocodilian fossils discussed in this paper, their identifications in previous papers, and their identification in this paper.

Specimen	Description	Identification in Willis 1997	Identification in Stein et al. 2016	Identification in this paper
QM F31060	rostrum	*Baru huberi* (holotype)	-	*Ultrastenos huberi,* probably the same individual as QM F31076.
QM F31061	right premaxilla and incomplete right maxilla	*Baru huberi* (paratype)	-	*Ultrastenos huberi*
QM F31062	right premaxilla	*Baru huberi* (paratype)	-	*Baru wickeni*
QM F31063	right maxilla fragment	*Baru huberi* (paratype)	-	*Baru wickeni*
QM F31064	right maxilla fragment	*Baru huberi* (paratype)	-	*Ultrastenos huberi*
QM F31068	left dentary fragment	*Baru huberi* (paratype)	-	*Ultrastenos huberi*
QM F31069	symphyseal fragment of mandible	*Baru huberi* (paratype)		*Ultrastenos huberi*
QM F31075	posterior cranial fragment	White Hunter Cranial Form 1	*Ultrastenos willisi*	*Ultrastenos huberi*
QM F31076	posterior cranial table	White Hunter Cranial Form 1	*Ultrastenos willisi*	*Ultrastenos huberi,* probably the same individual as QM F31060
QM F31079	posterior cranial fragment	White Hunter Cranial Form 2	-	*Quinkana meboldi*
QM F42665	posterior cranial and mandibular fragments fragments	-	*Ultrastenos willisi* (holotype)	*Ultrastenos huberi*
QM F61096	articulated left and right dentaries	-	-	*Ultrastenos huberi*
QM F61097	cranial fragment	-	-	*Ultrastenos huberi*

(Daudin, 1801) where this proportion ranges from 1.17 to 1.39 (Rio and Mannion, 2021: supplementary file 23). Lastly, the homodont dentition displayed by the last four teeth preserved in QM F42665 is simply insufficient to demonstrate homodonty of the entire dentition, a fact recognized by Stein et al. (2016b) themselves.

With the removal of *Ultrastenos* from the slender longirostrine category, it is worth examining the apparent absence of slender longirostry in any other currently known mekosuchine.

The Middle Miocene *H. camfieldensis* probably belongs in the slender longirostral category, although much of the rostrum is missing from the type, and only known, specimen (Megirian et al., 1991). It has been suggested to be a mekosuchine (Willis, 1997) and has been found to occupy a position at the base of (Stein et al., 2016b), or within (Iijima et al., 2022), Mekosuchinae in some phylogenetic analyses. However, the known remains of *H. camfieldensis* do not display any derived condition of Mekosuchinae that is not also widespread in non-mekosuchines (A.M. Yates pers. obs. of NTM P87106-1). The most recent phylogenetic analyses that have included: a) first hand observations of *H. camfieldensis*; b) a broad sample of mekosuchines based on first hand observations; and c) a broad range on non-mekosuchines are those of Lee and Yates (2018) and Ristevski et al. (2020, 2021, 2023a, b). These analyses fail to place *H. camfieldensis* within, or even close to, Mekosuchinae although they disagree on its actual position. Lee and Yates (2018), Ristevski et al. (2023a), and Ristevski et al. (2023b, with implied weighting in effect) found it to be a gavialid. Without implied weighting, Ristevski et al. (2023b) resolved it as a basal gavialoid, while the previous analyses based on older versions of the Ristevski dataset (Ristevski et al., 2020, 2021) found it to be a basal crocodyloid. Despite these disagreements there is little evidence that *H. camfieldensis* is a mekosuchine and mounting evidence that it is not.

It is remarkable that Mekosuchinae did not, to our knowledge, evolve a slender longirostrine ecomorphotype, despite exploring multiple morphotypic categories (as outlined in the introduction). This is not without precedent in crocodylian evolution. Alligatoroidea is a very diverse and long-lived crocodylian clade, occupying multiple ecomorphological categories that has failed to produce any truly slender longirostrines (Brochu, 2001; Drumheller and Wilberg, 2020). The reasons for this may lie with developmental constraints that reduce the number of possible ontogenetic trajectories that Alligatoroidea can exploit (Drumheller and Wilberg, 2020). It is possible that Mekosuchinae may have been similarly constrained by their ontogenetic pathways, although there is currently no evidence to support this speculation.

An alternative explanation might lie in the degree to which piscivory was employed within Australian Cenozoic ecosystems by non-mekosuchine taxa, or indeed the capacity of these ecosystems to support piscivory in general. Either possibility could present a barrier to Mekosuchinae entering into the longirostral part of morphospace, which is strongly associated with the piscivore role (Drumheller and Wilberg, 2020). The Australian record of slender longirostral crocodylians consists of four temporally separated taxa, spread temporally from the Eocene to the present across a wide geographic area. Firstly, there is a single fragment of a dentary symphysis of uncertain systematic position from the Eocene Corinda Formation of Runcorn, Queensland (Willis and Molnar, 1991b). The fragment is unlikely to belong to the clade that includes all presently recognized gavialoids because, although it is narrow, it has a short mandibular symphysis that does not extend posterior to the sixth dentary alveolus and lacks a splenial symphysis (Willis and Molnar, 1991b; Ristevski et al., 2023a, fig. 22b). Secondly, there is the aforementioned *H. camfieldensis* from the Middle Miocene of the Northern Territory. Thirdly, there is *Gunggamarandu maunala* Ristevski et al., 2021, a 'tomistomine' gavialid from the Pliocene or Pleistocene of the Darling Downs in Queensland, which is known from a single posterior cranial fragment. Finally, there is the extant *C. johnstoni*, which is also known as a fossil from the late Pleistocene of Queensland (Willis and Archer, 1990). Whether this record can be taken to literally reflect a sporadic and rare occupation of the slender longirostral ecomorph in the Cenozoic of Australia, or if it hints at successive, but poorly sampled, guilds of Australian longirostral piscivores is currently an unanswerable question.

ACKNOWLEDGEMENTS

We thank K. Spring and S. Hocknull of the Queensland Museum, in addition to A. Rackham of the Outback at Isa Community Center for facilitating access to the collection in their care. We also thank A. Gillespie and T. Myers of the University of New South Wales for their assistance in preparing several specimens. J. Ristevski kindly made available one of his own images for use in figure 18. We thank J. Ristevski and three other anonymous reviewers for their thoughtful reviews which improved the quality of this paper.

REFERENCES

Archer, M., Hand, S.J., Godthelp, H., and Creaser, P. 1997. Correlation of the Cainozoic sediments of the Riversleigh World Heritage fossil property, Queensland, Australia, p. 131–152. In Aguilar, J.P., Legendre, S., and Michaux, J. (eds.), Actes du Congrès BiochroM'97. Mémoires et Travaux de l'École Pratique des Hautes Études 21, Montpellier.

Arena, D.A., Travouillon, K.J., Beck, R.M.D., Black, K.H., Gillespie, A.K., Myers, T.J., Archer, M., and Hand, S.J. 2015. Mammalian lineages and the biostratigraphy and biochronology of Cenozoic faunas from the Riversleigh World Heritage Area, Australia. Lethaia, 49(1):43–60. https://doi.org/10.1111/let.12131

Ballell, A., Moon, B.C., Porro, L.B., Benton, M.J., and Rayfield, E.J. 2019. Convergence and functional evolution of longirostry in crocodylomorphs. Palaeontology, 62:867–887. https://doi.org/10.1111/pala.12432

Balouet, J.C. and Buffetaut, E. 1987. *Mekosuchus inexpectatus*, n. g., n. sp., Crocodilien nouveau de l'Holocène de Nouvelle Calédonie. Comptes rendus de l'Académie des sciences. Série 2, Mécanique, Physique, Chimie, Sciences de l'univers, Sciences de la Terre, 304(14):853–856.

Brochu, C.A. 1999. Phylogenetics, taxonomy, and historical biogeography of Alligatoroidea. Journal of Vertebrate Paleontology, 19(S2):9–100. https://doi.org/10.1080/02724634.1999.10011201

Brochu, C.A. 2001. Crocodylian snouts in space and time: phylogenetic approaches toward adaptive radiation. American Zoologist, 41:564–585. https://doi.org/10.1093/icb/41.3.564

Brochu, C.A. 2012. Phylogenetic relationships of Palaeogene ziphodont eusuchians and the status of *Pristichampsus* Gervais, 1853. Earth and Environmental Science Transactions of the Royal Society of Edinburgh, 103:521–550. https://doi.org/10.1017/S1755691013000200

Busbey, A.B. 1995. The structural consequences of skull flattening in crocodilians, p. 173–192. In Thomason, J.J. (ed.), Functional Morphology in Vertebrate Paleontology. Cambridge University Press, Cambridge.

D'Amore, D.C., Harmon, M., Drumheller, S.K., and Testin, J.J. 2019. Quantitative heterodonty in Crocodylia: assessing size and shape across modern and extinct taxa. PeerJ, 7(4):e6485. https://doi.org/10.7717/peerj.6485.

Daudin, F.M. 1801. Histoire Naturelle, Générale et Particulière des Reptiles; ouvrage faisant suit à l'Histoire naturell avants et particulière, composée par Leclerc de Buffon; et rédigee par C.S. Sonnini, avant de plusieurs sociétés avants. Vol. 2. F. Dufart, Paris.

Drumheller, S.K. and Wilberg, E.W. 2020. A synthetic approach for assessing the interplay of form and function in the crocodyliform snout. Zoological Journal of the Linnean Society, 188:507–521. https://doi.org/10.1093/zoolinnean/zlz081

Erickson, G.M., Gignac, P.M., Steppan, S.J., Lappin, A.K., Vliet, K.A., Brueggen, J.D., Inouye, B.D., Kledzik, D., and Webb, G.J.W. 2012. Insights into the ecology and evolutionary success of crocodilians revealed through bite-force and tooth-pressure experimentation. PLoS ONE, 7(3):e31781. https://doi.org/10.1371/journal.pone.0031781

Gillespie, A.K., Archer, M., and Hand, S.J. 2019. A new Oligo–Miocene marsupial lion from Australia and revision of the family Thylacoleonidae, Journal of Systematic Palaeontology, 17(1):59–89. https://doi.org/10.1080/14772019.2017.1391885

Gmelin, J.F. 1789. Systema Naturae, per regna tria Natura: secundum Classes, Ordines, Genera, Species, cum Characteribus, Differentiis, Synonymis, Locis. Tome 1, pars II. Leipzig, Lyon.

Graves, M.L. 1819. Sur deux nouvelles espèces de crocodile. Annales de la Société scientifique de Bruxelles, 2:343–353.

Iijima, M. 2017. Assessment of trophic ecomorphology in non-alligatoroid crocodylians and its adaptive and taxonomic implications. Journal of Anatomy, 231:192–211. https://doi.org/10.1111/joa.12626

Iijima, M., Qiao, Y., Lin, W., Peng, Y., Yoneda, M., and Liu, J. 2022. An intermediate crocodylian linking two extant gharials from the Bronze Age of China and its human induced extinction. Proceedings of the Royal Society B: Biological Sciences, 289:20220085. https://doi.org/10.1098/rspb.2022.0085

Krefft, G. 1873. Remarks on Australian crocodiles and description of a new species. Proceedings of the Zoological Society of London, 1873(II):334–335.

Lee, M.S. and Yates, A.M. 2018. Tip-dating and homoplasy: reconciling the shallow molecular divergences of modern gharials with their long fossil record. Proceedings of the Royal Society B: Biological Sciences, 285:20181071. https://doi.org/10.1098/rspb.2018.1071

Megirian, D. 1994. A new species of *Quinkana* Molnar (Eusuchia: Crocodylidae) from the Miocene Camfield Beds of northern Australia. The Beagle, Records of the Museums and Art Galleries of Northern Territory, 11:145–166.

Megirian, D., Murray, P.F., and Willis, P. 1991. A new crocodile of the gavial ecomorph morphology from the Miocene of northern Australia. The Beagle, Records of the Northern Territory Museum of Arts and Sciences, 8(1):135–158.

Molnar, R.E. 1982. Pleistocene ziphodont crocodilians of Queensland. Records of the Australian Museum, 33:803–834. https://doi.org/10.3853/j.0067-1975.33.1981.198

Montefeltro, F.C., Andrade, D.V., and Larsson, H.C. 2016. The evolution of the meatal chamber in crocodyliforms. Journal of Anatomy, 228(5):838–863. https://doi.org/10.1111/joa.12439

Müller, S. 1838. Waarnemingen over de Indische Krokodillen en Beschrijving Van Enne Nieuwe Soort. Tijdschrift voor Natuurlijke Geschiedenis en Physiologie, 5:61–87.

Myers, T.J. and Archer, M. 1997. *Kuterintja ngama* (Marsupialia, Ilariidae): a revised systematic analysis based on material from the late Oligocene of Riversleigh, northwestern Queensland. Memoirs of the Queensland Museum, 41:379–392.

Myers, T.J., Black, K.H., Archer, M., and Hand, S.J. 2017. The identification of Oligo–Miocene mammalian palaeocommunities from the Riversleigh World Heritage Area, Australia and an appraisal of palaeoecological techniques. PeerJ, 5:e3511. https://doi.org/10.7717/peerj.3511

Rio, J.P. and Mannion, P.D. 2021. Phylogenetic analysis of a new morphological dataset elucidates the evolutionary history of Crocodylia and resolves the long-standing gharial problem. PeerJ, 9:e12094. https://doi.org/10.7717/peerj.12094

Ristevski, J. 2022a. New insights into the taxonomic diversity and evolution of crocodylians from the Cenozoic Era of Australia. Unpublished PhD Thesis, University of Queensland, Brisbane, Australia

Ristevski, J. 2022b. Inside the head of one of the smallest crocodylians: paleoecological insights from the neuromorphology of *Trilophosuchus rackhami*, and tracing the origins of Mekosuchinae. Journal of Vertebrate Paleontology, Program and Abstracts, 2022:297–298.

Ristevski, J., Yates, A.M., Price, G.J., Molnar, R.E., Weisbecker, V., and Salisbury, S.W. 2020. Australia's prehistoric 'swamp king': revision of the Plio-Pleistocene crocodylian genus *Pallimnarchus* de Vis, 1886. PeerJ, 8**:**e10466. https://doi.org/10.7717/peerj.10466

Ristevski, J., Price, G.J., Weisbecker, V., and Salisbury, S.W. 2021. First record of a tomistomine crocodylian from Australia. Scientific Reports, 11:12158. https://doi.org/10.1038/s41598-021-91717-y

Ristevski, J., Willis, P.M.A., Yates, A.M., White, M., Hart, L., Stein, M.D., Price, G.J., and Salisbury, S.W. 2023a. Migrations, diversifications, and extinctions: the evolutionary history of crocodyliforms in Australasia. Alcheringa: An Australasian Journal of Palaeontology, 47:370–415. https://doi.org/10.1080/03115518.2023.2201319

Ristevski, J., Weisbecker, V., Scanlon, J.D., Price, G.J., and Salisbury, S.W. 2023b. Cranial anatomy of the mekosuchine crocodilian *Trilophosuchus rackhami* Willis, 1993. The Anatomical Record, 306(2):239–297. https://doi.org/10.1002/ar.25050

Rossmann, T. 2000. Skelettanatomische Beschreibung von *Pristichampus rollinatii* (Gray) (Crocodilia, Eusuchia) aus dem Paläogen von Europa, Nordamerika und Ostasien. Courier Forschungsinstitut Senckenberg, 221:1–107.

Salisbury, S.W and Willis, P.M.A. 1996. A new crocodylian from the Early Eocene of south-eastern Queensland and a preliminary investigation of the phylogenetic relationships of crocodyloids. Alcheringa: An Australasian Journal of Palaeontology, 20(3):179–226. https://doi.org/10.1080/03115519608619189

Scanlon, J.D. 2014. Giant terrestrial reptilian carnivores of Cenozoic Australia, p. 29–53. In Glen, A. and Dickman, C. (eds.), Carnivores of Australia. CSIRO Publishing, Clayton.

Stein, M., Archer, M., and Hand, S.J. 2016a. Dwarfism and feeding behaviours in Oligo–Miocene crocodiles from Riversleigh, northwestern Queensland, Australia. Acta Palaeontologica Polonica, 61(1):135–142. https://doi.org/10.4202/app.00134.2014

Stein, M., Hand, S.J., and Archer, M. 2016b. A new crocodile displaying extreme constriction of the mandible, from the late Oligocene of Riversleigh, Australia. Journal of Vertebrate Paleontology, 36(5):e1179041. https://doi.org/10.1080/02724634.2016.1179041

Travouillon, K., Archer, M., Hand, S.J., and Godthelp, H. 2006. Multivariate analyses of Cenozoic mammalian faunas from Riversleigh, northwestern Queensland. Alcheringa: An Australasian Journal of Palaeontology, 30(S1):323–349.

Willis, P.M.A. 1993. *Trilophosuchus rackhami* gen. et sp. nov., a new crocodilian from the early Miocene limestones of Riversleigh, northwestern Queensland. Journal of Vertebrate Paleontology, 13(1):90–98. https://doi.org/10.1080/02724634.1993.10011489

Willis, P.M.A. 1995. Crocodiles? Where? Look! - Up in the trees! Riversleigh Notes, 26:8–9.

Willis, P.M.A. 1997. New crocodilians from the late Oligocene White Hunter Site, Riversleigh, northwestern Queensland. Memoirs of the Queensland Museum, 41(2):423–438.

Willis, P.M.A. 2001. New crocodilian material from the Miocene of Riversleigh (northwestern Queensland, Australia), p. 64–74. In Grigg, G.C., Seebacher, F., and Franklin, C.E. (eds.), Crocodilian Biology and Evolution. Surrey Beatty and Sons, Sydney.

Willis, P.M.A. and Archer, M. 1990. A Pleistocene longirostrine crocodilian from Riversleigh: first fossil occurrence of *Crocodylus johnstoni* Krefft. Memoirs of the Queensland Museum, 28(1):159–163

Willis, P.M.A., Murray, P.F., and Megirian, D. 1990. *Baru darrowi* gen. et sp. nov., a large broad snouted crocodyline (Eusuchia: Crocodylidae) from mid-Tertiary freshwater limestones in northern Australia. Memoirs of the Queensland Museum, 29:521–540.

Willis, P.M.A. and Molnar, R.E. 1991a. A new middle Tertiary crocodile from Lake Palankarinna, South Australia. Records of the South Australian Museum, 25:39–55.

Willis, P.M.A. and Molnar, R.E. 1991b. A longirostrine crocodile from the Early Tertiary of southeastern Queensland. Alcheringa: An Australasian Journal of Palaeontology, 15:229–233. https://doi.org/10.1080/03115519108619019

Willis, P.M.A., Molnar, R.E., and Scanlon, J.D. 1993. An early Eocene crocodilian from Murgon, southeastern Queensland. Kaupia, 3:27–33.

Yates, A.M. 2017. The biochronology and palaeobiogeography of *Baru* (Crocodylia: Mekosuchinae) based on new specimens from the Northern Territory and Queensland. Australia PeerJ, 5:e3458. https://doi.org/10.7717/peerj.3458

Yates, A.M. and Pledge, N.S. 2017. A Pliocene mekosuchine (Eusuchia: Crocodilia) from the Lake Eyre Basin of South Australia. Journal of Vertebrate Paleontology, 37(1):e1244540. https://doi.org/10.1080/02724634.2017.1244540

Yates, A.M., Ristevski, J., and Salisbury, S.W. 2023. The last *Baru* (Crocodylia: Mekosuchinae): A new species of ‘clever headed crocodile’ from central Australia and a turnover of crocodylians during the late Miocene in Australia. Papers in Palaeontology, 9:e1523. https://doi.org/10.1002/spp2.1523